Electronic Supplementary Material (ESI) for Chemical Communications.

Electronic Supplementary Information for

Flow through Negatively Charged, Nanoporous Membranes Separates Li^+ and K^+

Chao Tang[a], Andriy Yaroshchuk[b,c,], and Merlin L. Bruening[a,d,*]

[a] Department of Chemical and Biomolecular Engineering, University of Notre Dame, Notre Dame, Indiana 46556, United States

[b] ICREA, pg·L.Companys 23, 08010 Barcelona, Spain

[c] Department of Chemical Engineering, Polytechnic University of Catalonia, av. Diagonal 647,08028 Barcelona, Spain

[d] Department of Chemistry and Biochemistry, University of Notre Dame, Notre Dame, Indiana 46556, United States

*Corresponding author: Merlin L. Bruening E-mail: mbruenin@nd.edu

Table of Contents

S1. Experimental methods

S1.1. Materials

Lithium chloride (crystal, ACS reagent) was purchased from Spectrum Chemical, and lithium hydroxide monohydrate (ACS reagent) and potassium chloride (BioXtra, ≥99.0%) were acquired from MilliporeSigma. Hydrophilic polycarbonate track-etched membranes (nominal 10 nm or 30 nm diameter pores, 47mm disk diameter, 6 µm thickness) and nylon membranes (1.2 µm pore size, 47 mm disk diameter) were obtained from Sterlitech. The track-etched membranes have a pore density of 6×10^8 pores/cm^2 with a tolerance of +/- 15%, according to the manufacturer. SEM images investigate only a fraction of a membrane, but they were consistent with a similar pore density around 8×10^8 pores/cm^2.[1] The burst strength of the track-etched membranes is 0.7 bar, per the manufacturer. K^+ and Li^+ standard solutions (TraceCert®, 1000 mg/L) were purchased from MilliporeSigma. All solutions were prepared with deionized water (Milli-Q Reference System, 18.2 MΩ cm).

S1.2. Membrane characterization

To estimate the pore size of the track-etched membranes, we obtained top-view membrane images using a Magellan 400 Scanning Electron Microscope (SEM). In determining the thickness of the membrane, a focused ion beam was used to section the membrane sample in the middle prior to SEM imaging of the membrane cross section (Helios G4 Ux Dual Beam instrument). Section S2 shows representative images.

S1.3. Separation experiments

All separations were carried out in a dead-end filtration unit (HP4750 stirred cell, Sterlitech) under various transmembrane pressures. The pressure was provided by a compressed nitrogen tank and adjusted with a pressure regulator. Unfortunately, the o-ring provided by the manufacture to prevent leakage was not suitable for these experiments, as the membrane broke when the operating pressure was above 120 psi. Instead, we made a flat o-ring seal from a Plumb Pak 6-in Rubber Washer pad (1/16-inch-thick) purchased from Lowe's. This homemade washer (Figure S1) showed excellent sealing while not damaging the membrane.

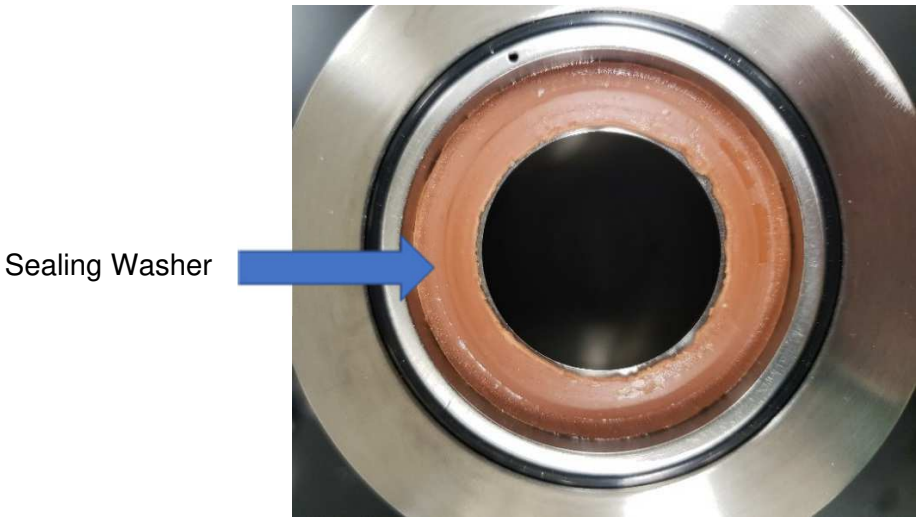

Figure S1. Photograph of the homemade seal (washer is bronze colored). This seal makes direct contact with the track-etched membrane.

A magnetic overhead stirrer, provided with the Sterlitech cell, was placed into the filtration unit and the cell was filled with 280 mL of feed solution. The cell was set on top of a magnetic stir plate, and the stirring speed was set at 1000 rpm. Despite the high rpm setting, the stirring was likely not effective near the cell wall, as noted in another study.[2] To reduce the stagnant area, all membranes were "masked" by a donut shaped piece of duct tape (Nashua dryer vent installation tape purchased from Home Depot). The mask had an open circular region in the middle with a radius of 1.55 cm, which reduced the membrane area active area to 7.55 cm^2. The outer diameter of the mask was 4.4 cm. All masks were cut using the Cricut Maker™ tool. To provide additional mechanical support, the membrane was placed on top of a nylon membrane (the tape mask was between the track-etched membrane and the nylon membrane). The whole assembly was then placed on top of a porous metallic support (Figure S2).

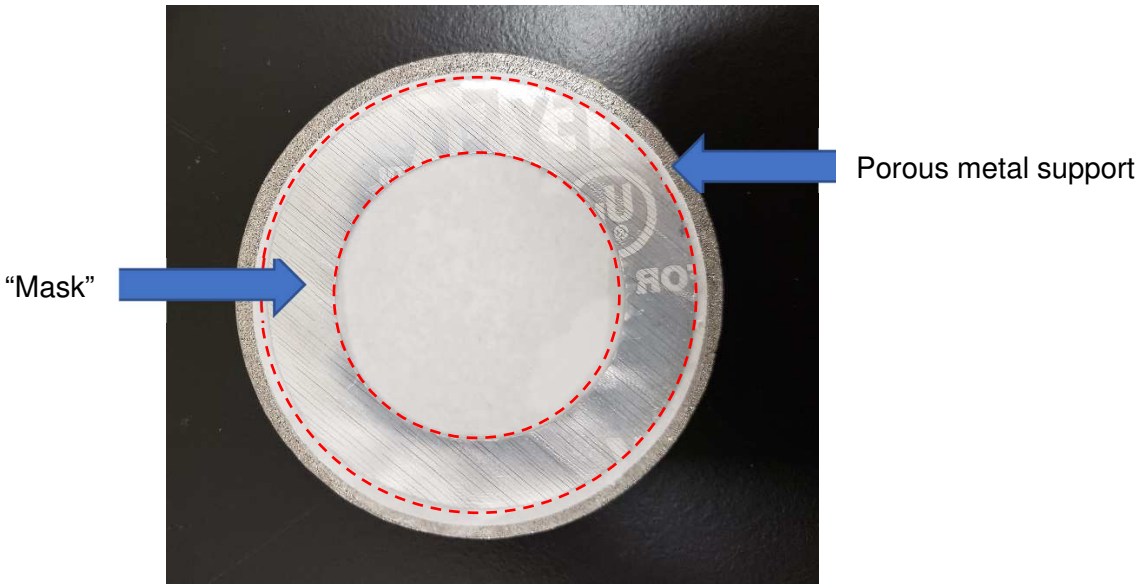

Figure S2. Photograph of the "masked" track-etched membrane supported by a nylon membrane on a porous metal support. The track-etched membrane is essentially transparent, so one can see the masking tape below it as well as the nylon membrane, which is only visible in the interior dashed circle. The tape "mask" resides between the track-etched membrane and nylon membrane, and the acrylic adhesive of the 'mask' should provide a tight seal.

Filtration through membranes with 30 nm pores: After assembly of the membranes in the stirred cell, 30 mL of feed solution was forced to pass through the membrane under a 13.8 bar transmembrane pressure with stirring. This step removes residual Na^+ in the membrane by replacing it with K^+ and Li^+. After this step, the stirred cell was depressurized and the remaining feed solution in the cell was discarded. The stirred cell was then refilled with feed solution and pressurized. The first 5 mL of permeate was discarded because steady state was likely not established. The next 5 mL of permeate was then collected as a sample. Permeates were collected in pristine 15-mL centrifuge tubes (Falcon™, polypropylene), and the time it took to collect 5 mL of permeate was recorded. The stirred cell was then depressurized and the remaining solution in the cell was discarded. The cell was then refilled with fresh feed solution and

pressurized to collect the next permeate sample at a different pressure (the first 5 mL of permeate was discarded again because steady state was likely not established yet). For each membrane, 3 permeates were collected at each transmembrane pressure. The experiment was performed with 2 different membranes, and reported error bars represent the standard deviations of 6 total measurements. We examined 3 feed solutions containing mixtures of lithium and potassium salts: 0.1 mM LiCl, 0.1 mM KCl; 0.1 mM LiOH, 0.1 mM KCl; and 0.5 mM LiOH, 0.5 mM KCl. Transmembrane pressures were selected in random orders (not from lowest to highest pressures) to avoid any possible changes in the membrane due to compaction at higher pressures. Tables S1-S6 present the experimental data with membranes containing 30 nm pores.

The permeate ion concentrations were determined using inductively coupled plasma - optical emission spectrometry (ICP-OES, PerkinElmer Optima 8000 or Avio 200). Calibration standards were made by diluting K^+ and Li^+ standard solutions (TraceCert®, 1000 mg/L) with 2% nitric acid. The passages of each ion were calculated using equation S1.

$$Passage = \frac{c_{i,permeate}}{c_{i,feed}} \times 100\% \quad \text{(S1)}$$

In the above equation, $c_{i,permeate}$ and $c_{i,feed}$ are the concentrations of ion i in the permeate and feed, respectively. In calculating the passage and selectivities, we used the designed feed concentrations, and analyses showed that the actual feed concentrations were within 5% of these values. The selectivity was calculated as the permeate concentration ratio divided by the feed concentration ratio, but the designed feed concentration ratio was always 1. Thus,

$$Li^+/K^+ \; Selectivity = \frac{c_{Li^+,permeate}}{c_{K^+,permeate}} \quad \text{(S2)}$$

The superficial velocity v (velocity with respect to the active membrane area, not inside the pore) was calculated by dividing the permeate volume V_p (5 mL) by the active membrane area A (7.55 cm^2) and time t (equation S3). Note that each membrane sample has slightly different pore density (+/- 15% tolerance). Therefore, the superficial velocity at a given pressure could differ by as much as 25% from sample to sample.

$$v = \frac{V_p}{At} \quad \text{(S3)}$$

Filtration through membranes with 10 nm pores: The experimental procedures for membranes with 10 nm pores are the same as for membranes with 30 nm pores, except for three changes. First, the rpm setting on the magnetic stir plate was set to 200 rpm (instead of 1000 rpm). This slows the nitrogen dissolution into the feed solution, which in turn reduces nitrogen passage through the membrane and formation of bubbles at the membrane outlet. Second, only 2 mL of permeate (instead of 5 mL) was collected for each sample (after passing 5 mL to approach steady state) to save time. The flow rate through membranes with 10 nm pores is more than an order of magnitude slower than that through 30 nm pores. Third, before the experiment, only 10 mL of feed solution was forced to pass through the membrane under a 27.6 bar transmembrane pressure with 200 rpm stirring. Table S7 presents the experimental data with membranes containing 10 nm pores.

Filtration through unmasked membranes: As previously mentioned, membranes were taped with a homemade duct tape "mask" (Figure S2) to minimize the membrane area near the cell wall where stirring was likely not effective and concentration polarization was severe. To demonstrate the effect of this "mask", we performed filtration experiments with unmasked membranes containing 30 nm pores and a 0.1 mM LiCl, 0.1 mM KCl feed mixture. The rpm setting on the magnetic stirrer plate was 1000 rpm as in other experiment with these membranes. We used relatively high transmembrane pressures (8.3, 11.0, and 13.8 bar) where concentration polarization is most evident. The experiment was performed with 2 different membranes, and reported error bars represent the standard deviations of 6 total measurements. Table S8 presents the experimental data with unmasked membranes and shows much lower selectivities without the tape (Figure S10).

Filtration with larger permeate volumes: To ensure that high Li^+/K^+ selectivities were not transient effects, we performed filtrations with much larger permeate volumes. For membranes containing 30 nm pores, we allowed 50% of the feed volume to permeate through the membranes in 5 mL aliquots and measured the Li^+ and K^+ concentrations in each aliquot. We performed this experiment with a 0.1 mM LiOH, 0.1 mM KCl feed mixture under 11.0 bar of transmembrane pressure. Under these conditions the Li^+/K^+ selectivity reached its maximum value of 70 when collecting only 5 mL of permeate (after discarding the first 5 mL). The experiment was performed with 2 different membranes, and each experiment lasted over 1 hour. For membranes containing 10 nm pores, we used a 0.5 mM LiOH, 0.5 mM KCl feed mixture under 27.6 bar of transmembrane pressure and collected 50 mL of permeate over more than 3 hours.

As the longer-term filtration experiments progress, the concentration in the remaining feed solution changes. For example, if the K^+ passage is 0, the feed K^+ concentration doubles after 50% of the feed volume passes through the membrane. Thus, we calculated the passage using equation (S4):

$$Passage = \frac{c_{i,permeate\ j}}{c_{i,feed\ j}} \times 100\% \quad \text{(S4)}$$

where $c_{i,permeate\ j}$ is the ion concentration of the jth permeate and $c_{i,feed\ j}$ is the arithmetic average feed concentration during the interval over which permeate j was collected. The corrected selectivity is:

$$Li^+/K^+\ Selectivity = \frac{Li^+,passage}{K^+,passage} \quad \text{(S5)}$$

Tables S9-S12 present the corrected feed concentrations, concentrations in each permeate, and corrected Li^+/K^+ selectivity.

S1.4. Stationary membrane potentials measurements

Stationary membrane potentials were measured using an apparatus described in our previous studies (Figure S3).[3] The potential difference between the two Ag/AgCl electrodes, $\phi^{Ag\prime} - \phi^{Ag}$, was measured with a digital multimeter. However, we are only interested in the potential difference across the membrane, $\phi^{S3} - \phi^{S2}$. Therefore, we need to measure or calculate the junction potentials, $\phi^{S2} - \phi^{S1}$ and $\phi^{S4} - \phi^{S3}$, and the potential differences in $(\phi^{Ag'} - \phi^{S4}) + (\phi^{S1} - \phi^{Ag})$. Note that $\phi^{S3} - \phi^{S2} = (\phi^{Ag'} - \phi^{Ag}) - (\phi^{Ag'} - \phi^{S4}) - (\phi^{S4} - \phi^{S3}) - (\phi^{S2} - \phi^{S1}) - (\phi^{S1} - \phi^{Ag})$.

To determine $(\phi^{Ag'} - \phi^{S4}) + (\phi^{S1} - \phi^{Ag})$, we put both Ag/AgCl electrodes in the receiving phase and measured the potential difference with a digital multimeter. To determine the junction potentials, $\phi^{S2} - \phi^{S1}$ and $\phi^{S4} - \phi^{S3}$, we employed the Henderson equation:

$$\phi^{\beta} - \phi^{\alpha} = \frac{\sum_i \frac{|z_i|}{z_i} u_i [c_i(\beta) - c_i(\alpha)]}{\sum_i |z_i| u_i [c_i(\beta) - c_i(\alpha)]} \frac{RT}{F} ln \frac{\sum_i |z_i| u_i c_i(\alpha)}{\sum_i |z_i| u_i c_i(\beta)} \quad \text{(S6)}$$

In the above equation, z_i, u_i, and c_i are the charge, electromobility, and concentration of ion i, respectively. α and β denote difference solution phases, and F, R, and T are Faraday's constant, the gas constant, and temperature, respectively.

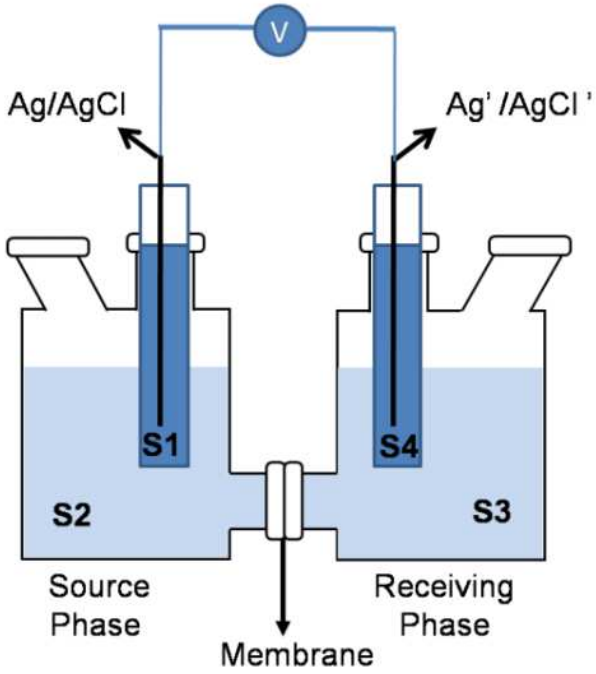

Figure S3. Experimental setup for stationary membrane potential measurements. Symbols S1 to S4 denote various KCl solutions separated by either frits or membranes. S1 and S4 are 3 M KCl solutions. S2 and S3 indicate the solutions in the source and receiving phases, respectively. Both source and receiving phases are stirred vigorously with magnetically driven stir bars, which are not shown in this diagram. The source phase contained 1.414 mM KCl solution and the receiving phase contained 0.707 mM KCl solution.

S2. Scanning electron microscopy (SEM) images

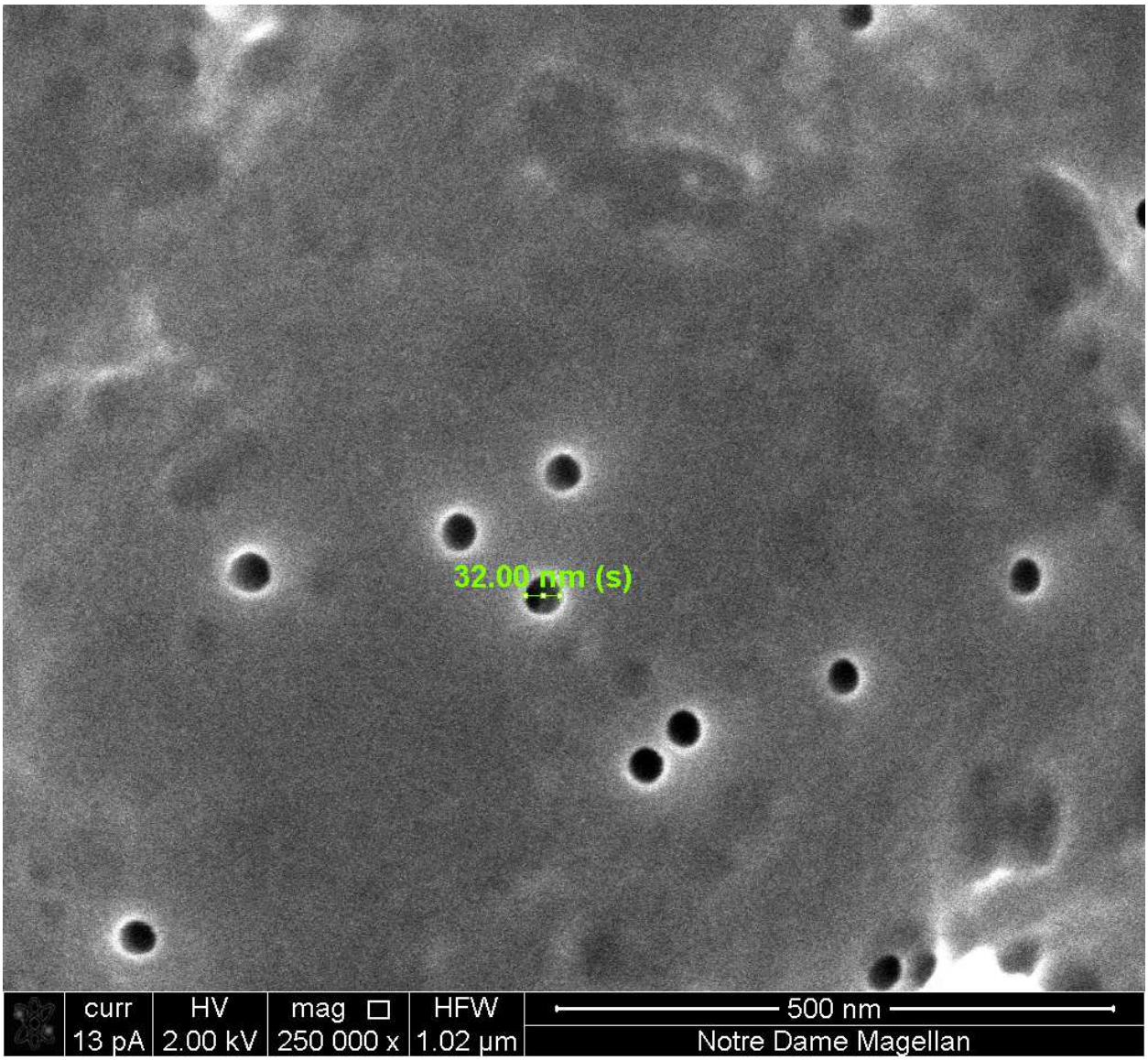

Figure S4. SEM image of a polycarbonate track-etched membrane (nominal 30 nm diameter pores).

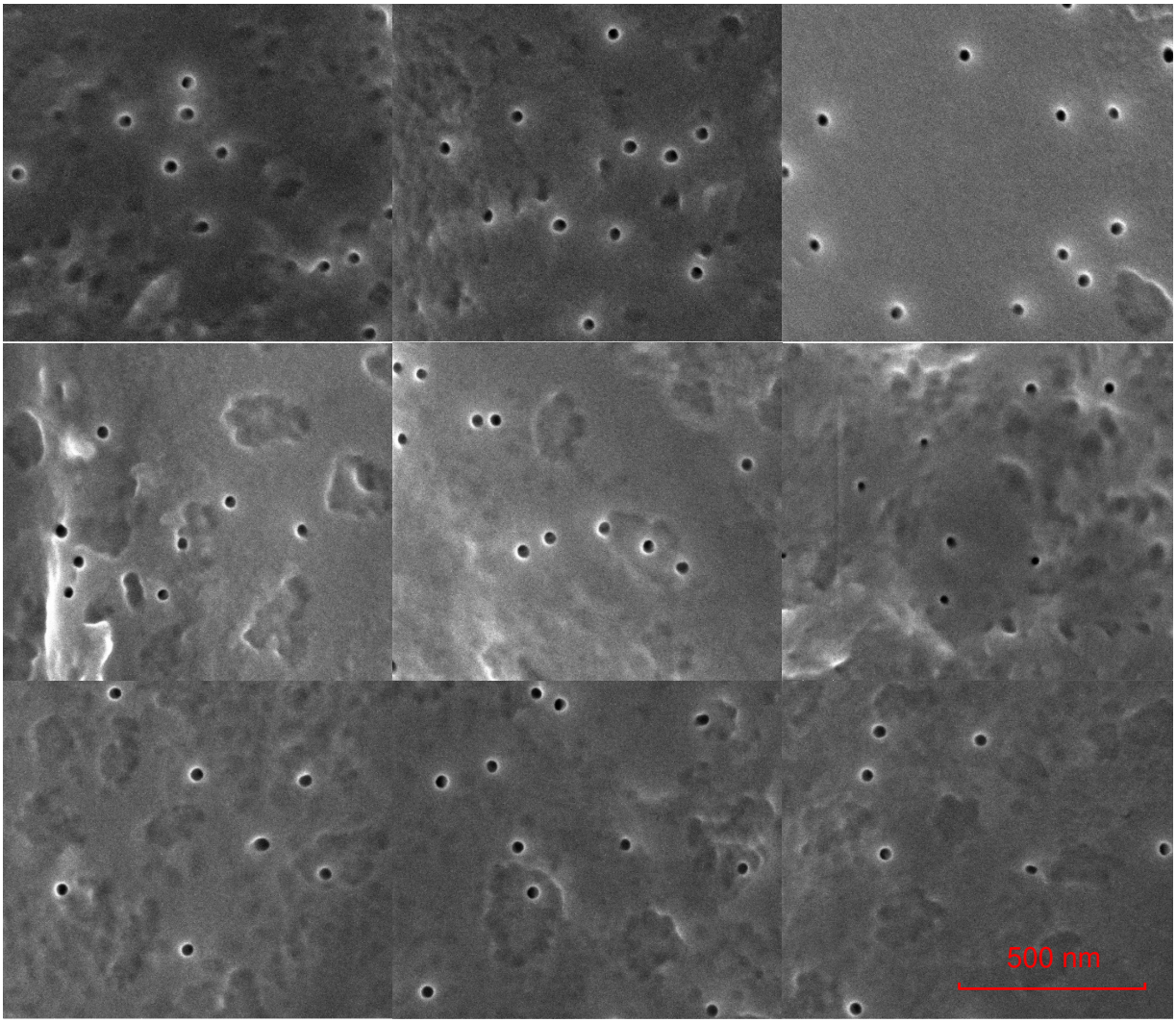

Figure S5. SEM images of polycarbonate track-etched membranes (nominal 30 nm diameter pores). 3 images are shown for 3 different membranes, where each row represents images from the same membrane. The scale bar is the same for all images.

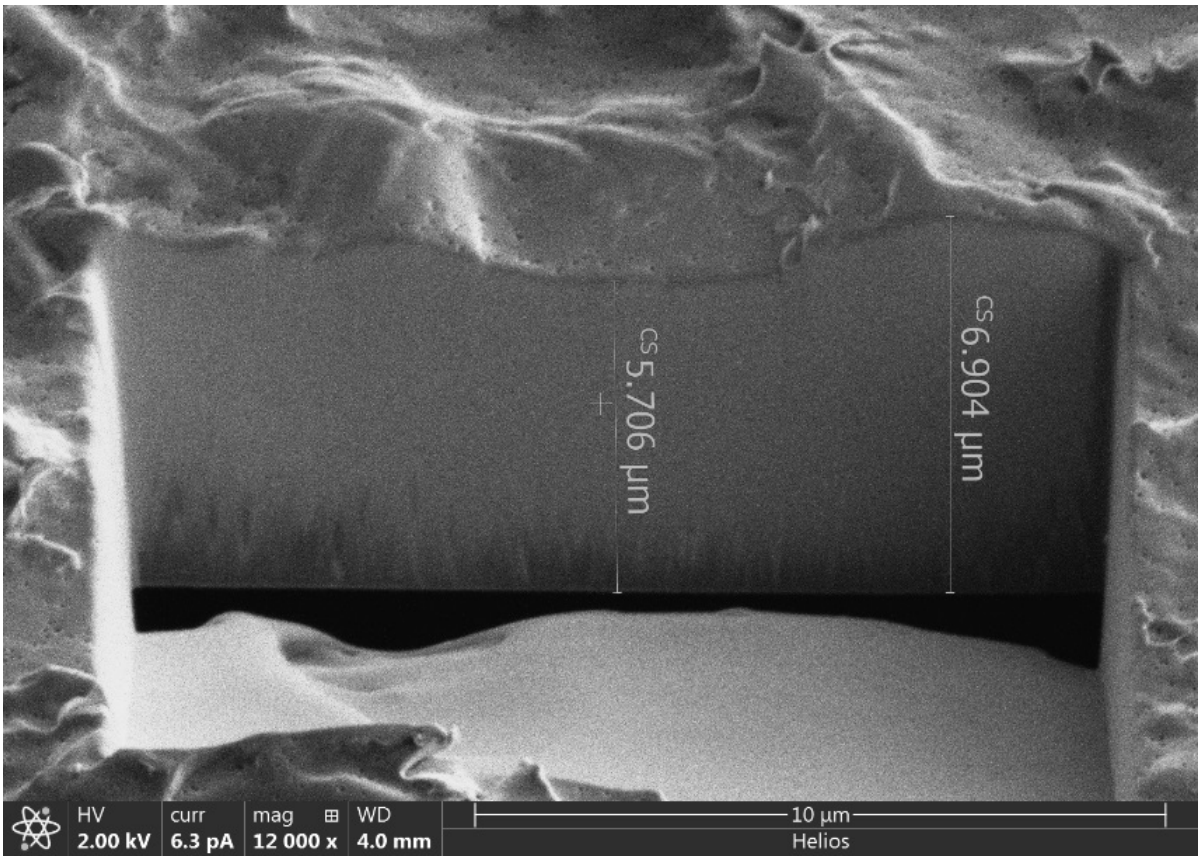

Figure S6. A side-view SEM image of a polycarbonate track-etched membrane (nominal 6 µm thickness). Measurements made in the image took the angle between the focal plane and the membrane surface normal into account.

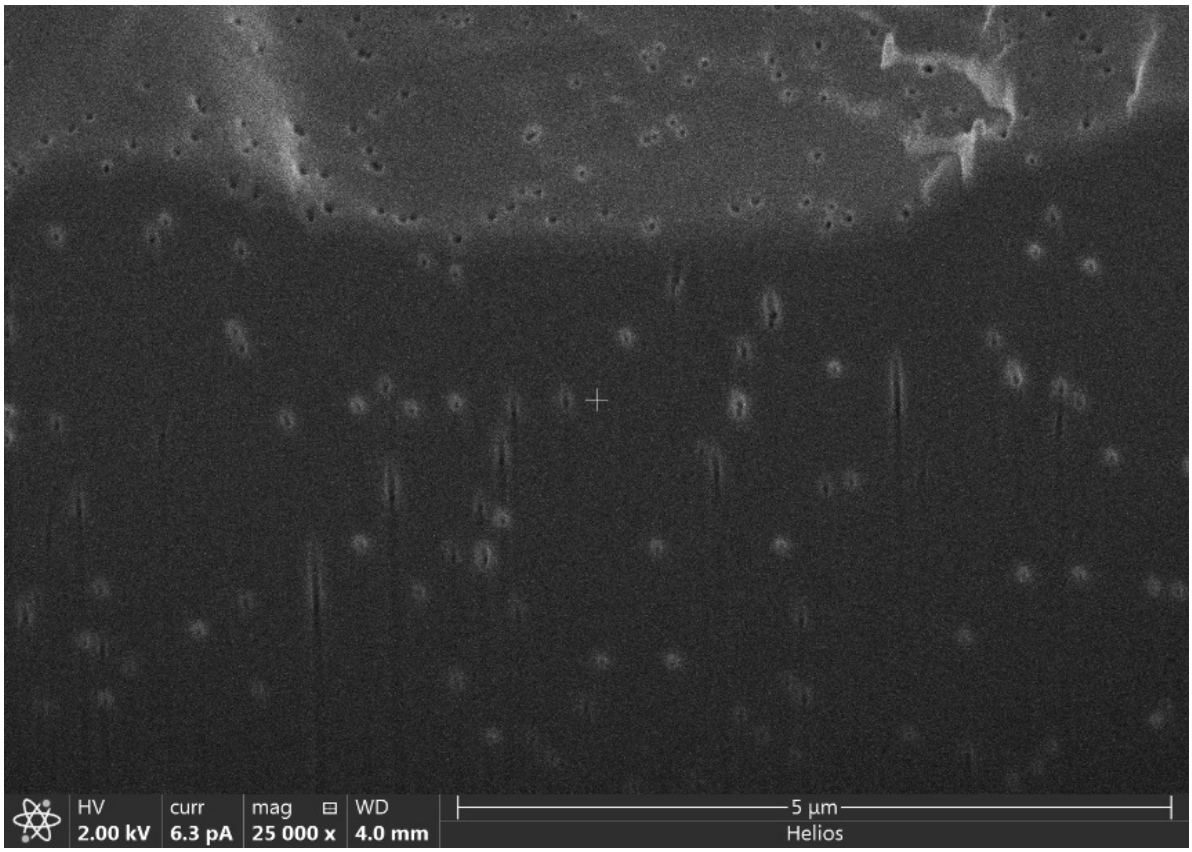

Figure S7. Cross-sectional SEM image of a polycarbonate track-etched membrane showing pores passing through the membrane.

S3. Experimental data

S3.1. Filtration through membranes with 30 nm pores

Table S1. K^+ and Li^+ passages and Li^+/K^+ selectivities during flow through a single polycarbonate track-etched membrane (nominal 30 nm pores) at various transmembrane pressures. The table also shows the superficial normal velocity above the membrane. The feed solutions contained a 0.1 mM LiCl, 0.1 mM KCl mixture. These are data for the first membrane sample. The experiments were performed in random order, not with sequentially increasing pressures.

Transmembrane Pressure in psig (**bar**)	K^+ passage %	Li^+ passage %	Selectivity	Superficial velocity (µm/s)
10 **(0.7)**	9.1	26.3	2.9	3.7
	8.3	20.6	2.5	3.7
	8.7	22.0	2.5	3.7
20 **(1.4)**	5.0	22.8	4.5	6.4
	5.0	22.0	4.4	6.2
	5.2	22.0	4.3	6.2
40 **(2.8)**	2.6	24.8	9.6	12.9
	2.5	22.9	9.2	13.0
	2.5	23.8	9.4	13.3
60 **(4.1)**	1.5	28.9	18.8	23.2
	1.5	30.9	20.5	24.0
	1.3	29.2	22.7	24.2
80 **(5.5)**	1.0	31.8	30.3	29.3
	1.1	32.1	28.4	28.7
	1.0	32.9	32.6	29.2
120 **(8.3)**	0.8	35.5	44.4	41.4
	0.8	36.5	43.6	41.1
	0.8	37.2	44.1	40.1
160 **(11.0)**	0.9	41.2	46.9	52.6
	0.9	32.5	35.2	53.4
	1.7	34.5	20.5	52.6
200 **(13.8)**	1.9	46.9	24.5	61.3
	1.9	46.7	24.4	64.3
	1.8	47.3	26.1	64.3

Table S2. K^+ and Li^+ passages and Li^+/K^+ selectivities during flow through a single polycarbonate track-etched membrane (nominal 30 nm pores) at various transmembrane pressures. The table also shows the superficial normal velocity above the membrane. The feed solutions contained a 0.1 mM LiCl, 0.1 mM KCl mixture. These are data for the second membrane sample. The experiments were performed in random order, not with sequentially increasing pressures.

Transmembrane Pressure in psig (**bar**)	K^+ passage %	Li^+ passage %	Selectivity	Superficial velocity (μm/s)
10 **(0.7)**	7.8	20.8	2.7	4.2
	7.8	21.0	2.7	4.1
	8.1	22.2	2.7	4.1
20 **(1.4)**	4.7	24.5	5.2	7.5
	4.5	22.7	5.0	7.5
	4.6	23.5	5.2	7.7
40 **(2.8)**	2.0	25.4	12.6	15.3
	2.0	25.8	12.6	14.9
	2.0	27.2	13.4	15.1
60 **(4.1)**	1.1	28.1	25.8	24.5
	1.1	28.8	26.0	25.0
	1.0	29.9	28.6	25.5
80 **(5.5)**	0.9	31.2	35.8	32.6
	0.8	32.1	38.1	33.0
	0.8	32.9	43.3	33.1
120 **(8.3)**	0.8	38.5	45.7	45.7
	0.8	38.7	49.9	45.7
	0.7	39.6	57.3	46.0
160 **(11.0)**	1.0	44.9	46.6	59.1
	0.9	45.3	50.9	60.2
	0.8	46.8	58.5	58.6
200 **(13.8)**	2.3	53.9	23.8	72.0
	1.5	53.9	35.9	72.8
	1.3	54.9	42.4	71.2

Table S3. K^+ and Li^+ passages and Li^+/K^+ selectivities during flow through a single polycarbonate track-etched membrane (nominal 30 nm pores) at various transmembrane pressures. The table also shows the superficial normal velocity above the membrane. The feed solutions contained a 0.1 mM LiOH, 0.1 mM KCl mixture. These are data for the first membrane sample. The experiments were performed in random order, not with sequentially increasing pressures.

Transmembrane Pressure in psig (**bar**)	K^+ passage %	Li^+ passage %	Selectivity	Superficial velocity (µm/s)
10 **(0.7)**	7.6	23.0	3.0	3.3
	9.5	22.2	2.3	3.2
	8.3	21.4	2.6	3.4
20 **(1.4)**	5.3	23.4	4.4	5.9
	4.8	23.5	4.9	5.9
	4.4	23.5	5.4	5.8
40 **(2.8)**	1.1	26.6	23.6	11.2
	1.4	26.9	19.7	11.6
	1.5	27.0	18.4	11.4
60 **(4.1)**	0.8	25.6	32.9	21.7
	0.8	25.5	31.5	21.7
	0.9	26.4	29.9	20.7
80 **(5.5)**	0.6	29.3	52.2	25.5
	0.5	30.9	60.7	26.3
	0.5	31.1	56.9	27.0
120 **(8.3)**	0.5	36.4	71.1	36.2
	0.7	35.6	53.5	35.8
	0.5	36.9	72.4	35.6
160 **(11.0)**	0.6	43.4	69.7	46.7
	0.4	43.9	100.1	46.7
	0.6	44.2	73.5	47.3
200 **(13.8)**	1.1	50.2	47.0	57.1
	0.8	50.8	60.7	58.1
	0.9	50.8	55.4	58.6

Table S4. K^+ and Li^+ passages and Li^+/K^+ selectivities during flow through a single polycarbonate track-etched membrane (nominal 30 nm pores) at various transmembrane pressures. The table also shows the superficial normal velocity above the membrane. The feed solutions contained a 0.1 mM LiOH, 0.1 mM KCl mixture. These are data for the second membrane sample. The experiments were performed in random order, not with sequentially increasing pressures.

Transmembrane Pressure in psig (**bar**)	K^+ passage %	Li^+ passage %	Selectivity	Superficial velocity (µm/s)
10 **(0.7)**	7.9	22.2	2.8	4.0
	8.5	22.4	2.6	3.9
	8.5	21.8	2.6	4.0
20 **(1.4)**	4.9	22.2	4.5	7.6
	4.8	21.9	4.6	7.6
	5.0	22.2	4.5	7.3
40 **(2.8)**	1.6	25.5	16.5	14.7
	1.7	25.6	15.3	14.4
	1.7	24.9	14.4	14.7
60 **(4.1)**	1.0	27.1	25.9	25.7
	0.9	27.6	30.9	25.7
	0.8	27.3	34.8	26.7
80 **(5.5)**	0.7	30.5	44.7	31.2
	0.6	30.4	48.9	31.7
	0.7	30.5	46.6	31.5
120 **(8.3)**	0.6	34.4	57.5	44.2
	0.5	35.3	67.9	43.3
	0.5	35.7	69.0	43.3
160 **(11.0)**	0.7	41.5	60.6	57.6
	0.7	43.8	62.1	58.6
	0.7	42.9	63.9	58.6
200 **(13.8)**	2.6	50.6	19.4	72.8
	2.5	49.7	19.8	73.6
	2.7	50.7	19.0	73.6

Table S5. K^+ and Li^+ passages and Li^+/K^+ selectivities during flow through a single polycarbonate track-etched membrane (nominal 30 nm pores) at various transmembrane pressures. The table also shows the superficial normal velocity above the membrane. The feed solutions contained a 0.5 mM LiOH, 0.5 mM KCl mixture. These are data for the first membrane sample. The experiments were performed in random order, not with sequentially increasing pressures.

Transmembrane Pressure in psig (**bar**)	K^+ passage %	Li^+ passage %	Selectivity	Superficial velocity (µm/s)
10 **(0.7)**	29.0	65.5	2.3	4.3
	31.6	68.6	2.2	4.3
	32.9	67.5	2.1	4.2
20 **(1.4)**	22.3	75.1	3.4	7.9
	21.4	76.1	3.5	8.1
	21.0	74.3	3.5	8.0
40 **(2.8)**	11.6	88.7	7.6	15.5
	10.6	85.8	8.1	15.3
	11.1	87.2	7.9	15.6
60 **(4.1)**	4.8	83.7	17.3	27.4
	4.3	85.2	20.0	27.7
	4.1	85.1	20.7	27.6
80 **(5.5)**	3.8	95.0	25.2	36.0
	3.6	94.3	26.0	35.2
	3.6	95.1	26.3	35.2
120 **(8.3)**	4.3	101.7	23.8	48.0
	4.6	104.3	22.7	49.8
	4.0	104.8	26.1	47.3
160 **(11.0)**	5.8	106.4	18.3	61.3
	5.9	107.8	18.2	62.5
	5.9	107.7	18.2	63.1
200 **(13.8)**	8.9	112.7	12.7	76.1
	8.3	113.4	13.6	77.0
	9.1	113.4	12.4	77.9

Table S6. K^+ and Li^+ passages and Li^+/K^+ selectivities during flow through a single polycarbonate track-etched membrane (nominal 30 nm pores) at various transmembrane pressures. The table also shows the superficial normal velocity above the membrane. The feed solutions contained a 0.5 mM LiOH, 0.5 mM KCl mixture. These are data for the second membrane sample. The experiments were performed in random order, not with sequentially increasing pressures.

Transmembrane Pressure in psig (**bar**)	K^+ passage %	Li^+ passage %	Selectivity	Superficial velocity (µm/s)
10 **(0.7)**	30.6	67.1	2.2	3.8
	30.4	66.5	2.2	3.7
	31.0	67.1	2.2	3.8
20 **(1.4)**	21.2	69.0	3.2	7.2
	22.1	72.3	3.3	7.0
	22.3	74.4	3.3	7.1
40 **(2.8)**	12.0	80.4	6.7	14.1
	11.9	80.1	6.7	14.2
	12.2	79.8	6.5	14.3
60 **(4.1)**	6.1	82.3	13.4	25.1
	6.2	83.2	13.5	25.6
	6.2	84.5	13.6	25.4
80 **(5.5)**	5.7	89.1	15.6	31.7
	5.7	90.0	15.8	30.5
	5.7	91.0	16.0	32.0
120 **(8.3)**	8.9	98.2	11.0	44.2
	6.8	98.5	14.4	44.8
	6.8	98.3	14.5	44.5
160 **(11.0)**	8.6	102.6	11.9	57.6
	8.4	102.9	12.3	56.6
	8.4	103.8	12.3	57.1
200 **(13.8)**	12.9	105.0	8.2	72.0
	12.7	106.0	8.3	71.2
	13.1	107.9	8.2	71.2

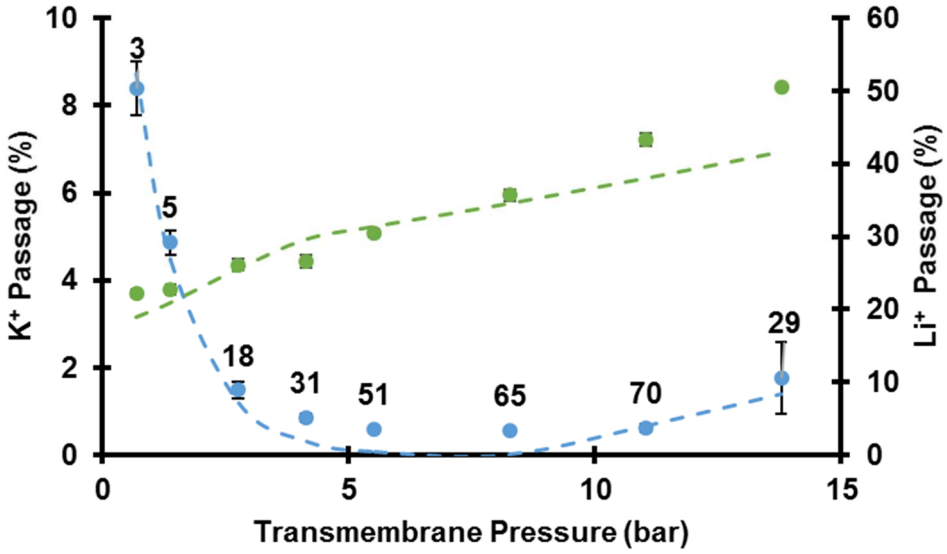

Figure S8. K^+ (blue, left y-axis) and Li^+ (green, right y-axis) passages during flow of a 0.1 mM KCl, 0.1 mM LiOH mixture through polycarbonate track-etched membranes (30 nm pores) using various transmembrane pressures. Dashed lines show simulation results with a linear combination of 10-µm (97%) and 75-µm (3%) unstirred layers. The simulation assumes a surface charge density of -5 mC/m^2. The numbers above K^+ passages are Li^+/K^+ selectivities at the given pressure. The experimental data are from Tables S3 and S4. Simulation results are from Table S17.

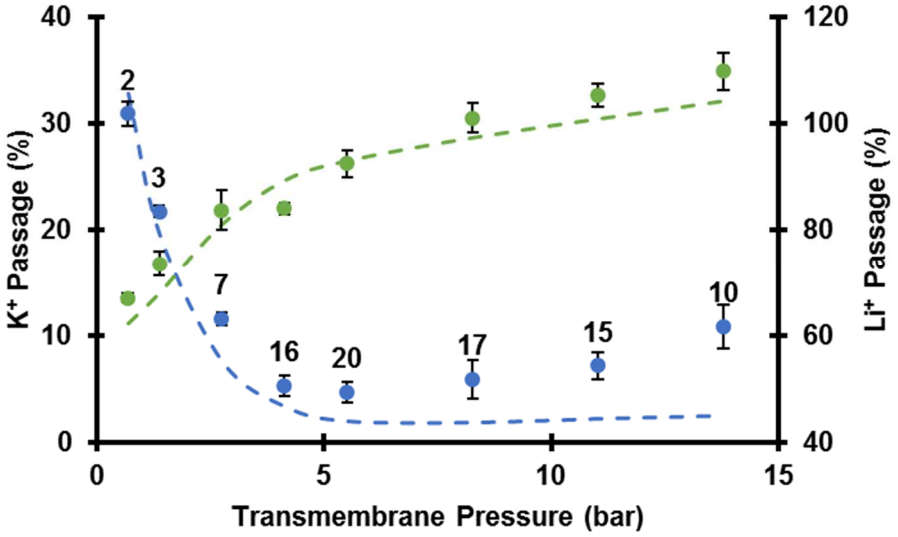

Figure S9. K^+ (blue, left y-axis) and Li^+ (green, right y-axis) passages during flow of a 0.5 mM LiOH, 0.5 mM KCl mixture through polycarbonate track-etched membranes (30 nm pores) using various transmembrane pressures. Dashed lines show simulation results with a linear combination of 10-µm (97%) and 75-µm (3%) unstirred layers. The simulation assumes a surface charge density of -7 mC/m^2. The numbers above K^+ passages are Li^+/K^+ selectivities at the given pressure. The experimental data are from Tables S5 and S6. Simulation results are from Table S18.

S3.2. Filtration through membranes with 10 nm pores

Table S7. K^+ and Li^+ passages and Li^+/K^+ selectivities during flow through a polycarbonate track-etched membrane (nominal 10 nm pore size) at 27.6 bar of transmembrane pressure. The feed solutions contained a 0.5 mM LiOH, 0.5 mM KCl mixture.

Membrane	K^+ passage %	Li^+ passage %	Selectivity
1	0.9	45.1	48.6
	0.9	46.6	52.5
	0.8	46.3	56.1
2	0.7	43.0	60.1
	0.6	43.9	69.3
	0.5	44.5	90.1

S3.3. Filtration through unmasked membranes

Table S8. K^+ and Li^+ passages and Li^+/K^+ selectivities during flow through **unmasked** polycarbonate track-etched membranes (nominal 30 nm pores) at various transmembrane pressures. The feed solutions contained a 0.1 mM LiCl, 0.1 mM KCl mixture. The experiments were performed in random order, not with sequentially increasing pressures. Tables S1 and S2 present results for masked membranes.

Membrane	Transmembrane Pressure in psig (**bar**)	K^+ passage %	Li^+ passage %	Selectivity
1	120 **(8.3)**	4.6	37.8	8.3
		4.2	37.9	9.0
		4.2	38.9	9.2
	160 **(11.0)**	6.4	54.0	8.4
		5.3	46.5	8.8
		4.7	46.4	9.9
	200 **(13.8)**	5.7	53.7	9.4
		4.2	55.7	13.1
		5.1	55.1	10.8
2	120 **(8.3)**	4.4	43.1	9.8
		4.1	34.5	8.3
		3.6	36.1	10.1
	160 **(11.0)**	4.5	41.9	9.4
		4.6	42.0	9.2
		3.8	44.5	11.6
	200 **(13.8)**	5.2	50.4	9.8
		4.2	52.4	12.5
		5.2	51.6	9.9

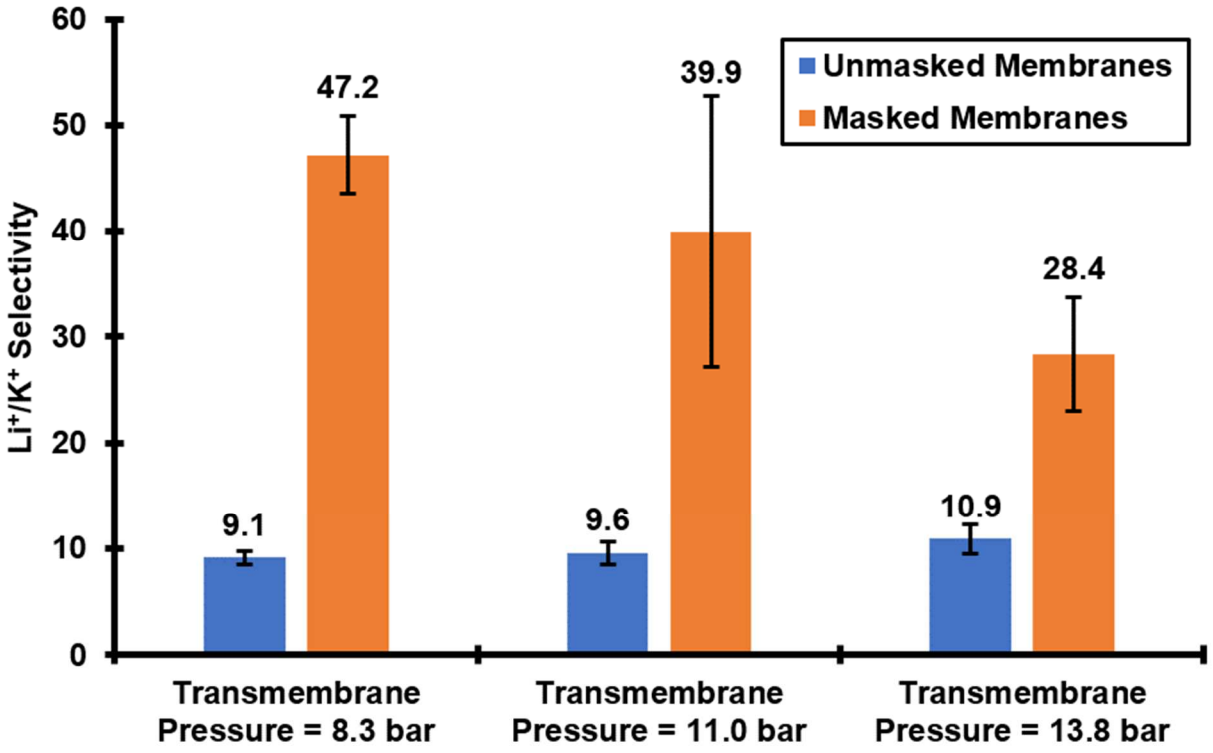

Figure S10. Comparison of Li^+/K^+ selectivities with tape-masked or unmasked membranes containing 30 nm pores (Tables S1, S2, and S8). The feed solution contained a 0.1 mM LiCl, 0.1 mM KCl mixture, and filtration occurred with various transmembrane pressures. Unmasked membranes exhibit much smaller selectivities due to undesired higher K^+ passages, which likely result from stagnant regions near the cell wall.

S3.4. Filtration with larger permeate volumes

Table S9. K^+ and Li^+ passages and Li^+/K^+ selectivities during flow through a polycarbonate track-etched membrane (nominal 30 nm pores) at 11.0 bar of transmembrane pressure. The feed solutions initially contained a 0.1 mM LiOH, 0.1 mM KCl mixture. These are data for the first membrane sample. The calculated passages account for the changing feed concentrations.

Permeate #	K^+ concentration in the feed (mM)	Li^+ concentration in the feed (mM)	K^+ passage %	Li^+ passage %	Selectivity
1	0.101	0.101	4.5	42.3	9.3
2	0.103	0.102	0.7	42.0	63.6
3	0.105	0.103	0.7	41.9	60.5
4	0.107	0.104	0.7	42.0	61.8
5	0.109	0.105	0.7	41.3	57.2
6	0.111	0.106	0.8	41.4	52.4
7	0.113	0.107	0.7	42.2	58.6
8	0.115	0.109	0.7	41.6	60.8
9	0.118	0.110	0.7	41.9	62.5
10	0.120	0.111	0.7	43.1	65.9
11	0.123	0.113	0.7	42.8	63.4
12	0.126	0.114	0.7	44.1	62.5
13	0.128	0.116	0.7	43.9	63.6
14	0.131	0.117	0.7	44.9	68.6
15	0.135	0.119	0.7	45.8	65.6
16	0.138	0.120	0.7	45.1	68.7
17	0.141	0.122	0.6	46.6	72.8
18	0.145	0.124	0.6	46.9	76.7
19	0.149	0.125	0.6	46.9	76.7
20	0.153	0.127	0.6	48.7	82.6
21	0.157	0.129	0.6	49.2	83.3
22	0.162	0.131	0.6	49.4	84.1
23	0.167	0.133	0.6	50.1	90.3
24	0.172	0.135	0.6	51.4	91.9
25	0.177	0.137	0.6	52.8	93.7
26	0.183	0.139	0.6	53.7	97.6
27	0.189	0.141	0.6	54.6	92.6
28	0.196	0.143	0.6	57.0	97.0

Table S10. K^+ and Li^+ passages and Li^+/K^+ selectivities during flow through a polycarbonate track-etched membrane (nominal 30 nm pores) at 11.0 bar of transmembrane pressure. The feed solutions initially contained a 0.1 mM LiOH, 0.1 mM KCl mixture. These are data for the second membrane sample. The calculated passages account for the changing feed concentrations.

Permeate #	K^+ concentration in the feed (mM)	Li^+ concentration in the feed (mM)	K^+ passage %	Li^+ passage %	Selectivity
1	0.101	0.101	5.2	40.2	7.8
2	0.103	0.102	0.8	42.7	56.2
3	0.105	0.103	0.7	42.5	56.8
4	0.107	0.104	0.7	42.9	59.7
5	0.109	0.105	0.8	42.8	55.3
6	0.111	0.106	0.8	42.7	56.2
7	0.113	0.107	0.8	42.6	56.0
8	0.115	0.109	0.7	42.7	58.9
9	0.118	0.110	0.7	43.6	63.9
10	0.120	0.111	0.7	43.8	63.6
11	0.123	0.113	0.7	45.0	66.5
12	0.126	0.114	0.7	46.6	68.8
13	0.128	0.115	0.7	45.6	69.8
14	0.131	0.117	0.7	47.1	71.5
15	0.135	0.118	0.6	48.0	76.7
16	0.138	0.120	0.7	48.4	71.7
17	0.141	0.121	0.6	49.1	83.2
18	0.145	0.123	0.6	48.9	82.8
19	0.149	0.125	0.6	49.5	82.7
20	0.153	0.126	0.6	50.9	89.4
21	0.157	0.128	0.6	52.1	87.2
22	0.162	0.130	0.6	52.4	81.6
23	0.166	0.132	0.6	53.9	91.6
24	0.172	0.133	0.6	54.5	93.3
25	0.177	0.135	0.6	55.7	89.7
26	0.183	0.137	0.6	55.7	90.6
27	0.189	0.139	0.6	57.7	89.3
28	0.196	0.141	0.7	58.2	84.4

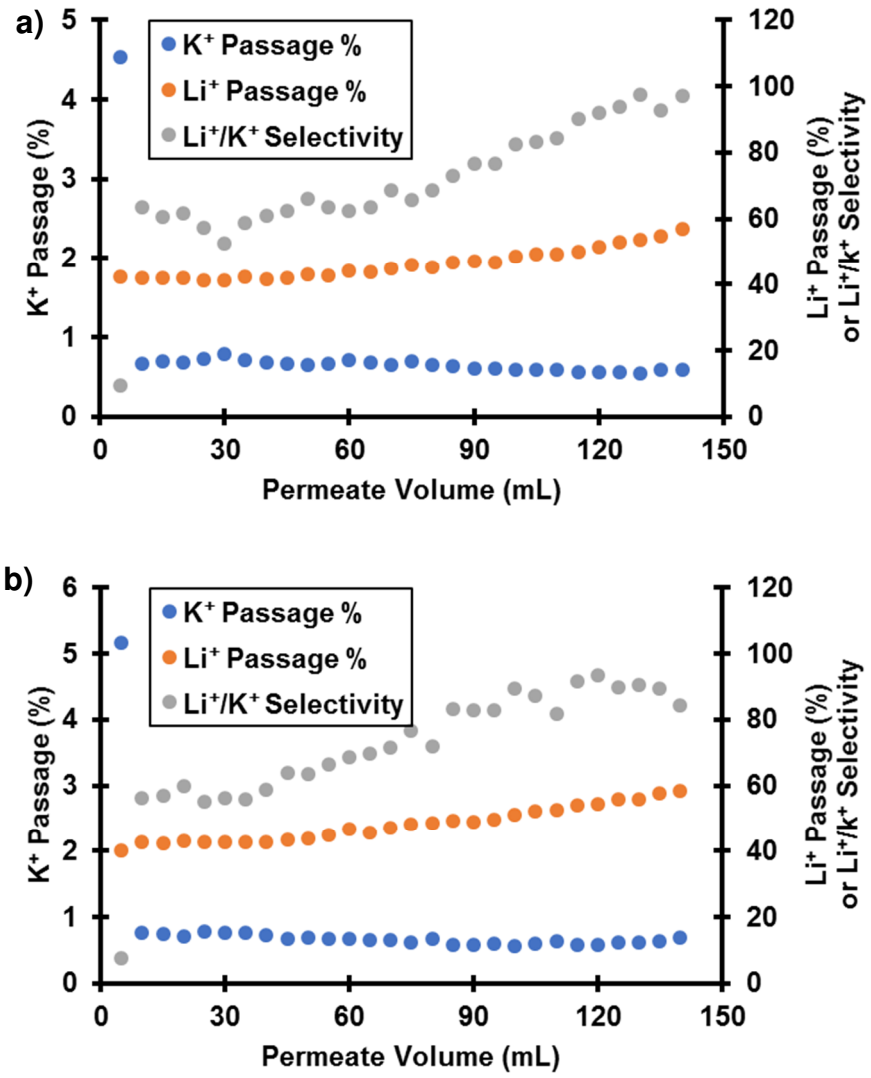

Figure S11. K^+ and Li^+ passages and Li^+/K^+ selectivities during flow through two different polycarbonate track-etched membrane samples (a and b) (nominal 30 nm pores) at 11.0 bar of transmembrane pressure. The feed initially contained a 0.1 mM LiOH, 0.1 mM KCl mixture. In typical experiments, we discard the first data point.

Tables S9 and S10 and Figure S11 show how K^+ and Li^+ passages and Li^+/K^+ selectivities evolve during passage of 50% of the feed solution through the membrane. Over this time, the feed ion concentrations change as much as 90% for K^+ and 40% for Li^+. Both the increasing ionic strength in the feed solution and the increasing K^+/Li^+ ratio should enhance the passages of both ions. However, the data show no significant increase in the K^+ passage, presumably because most passage occurs in poorly stirred regions with more severe concentration polarization. In contrast, Li^+ passage increases from 40.2% to at most 57.7% over the course of the experiment. Overall, these are relatively small changes in passage over the course of the filtration, indicating that experiments with small permeate volumes (10 mL total) represent a pseudo steady state.

Table S11. K^+ and Li^+ passages and Li^+/K^+ selectivities during flow through a polycarbonate track-etched membrane (nominal 10 nm pores) at 11.0 bar of transmembrane pressure. The feed solutions contained a 0.5 mM LiOH, 0.5 mM KCl mixture. These are data for the first membrane sample.

Permeate #	K^+ concentration in the feed (mM)	Li^+ concentration in the feed (mM)	K^+ passage %	Li^+ passage %	Selectivity
1	0.503	0.503	32.1	36.9	1.2
2	0.511	0.508	0.6	41.4	70.5
3	0.520	0.514	0.6	43.3	69.2
4	0.530	0.519	0.7	44.8	68.3
5	0.540	0.525	0.6	48.3	79.9
6	0.551	0.530	0.6	49.5	87.1
7	0.562	0.535	0.6	50.5	91.8
8	0.574	0.541	0.7	50.9	74.6
9	0.586	0.546	0.7	55.3	81.9
10	0.598	0.551	0.7	56.5	81.6

Table S12. K^+ and Li^+ passages and Li^+/K^+ selectivities during flow through a polycarbonate track-etched membrane (nominal 10 nm pores) at 11.0 bar of transmembrane pressure. The feed solutions contained a 0.5 mM LiOH, 0.5 mM KCl mixture. These are data for the second membrane sample.

Permeate #	K^+ concentration in the feed (mM)	Li^+ concentration in the feed (mM)	K^+ passage %	Li^+ passage %	Selectivity
1	0.504	0.502	21.7	51.6	2.4
2	0.512	0.507	0.7	40.1	57.0
3	0.521	0.513	0.7	40.8	61.2
4	0.531	0.518	0.7	43.3	65.5
5	0.541	0.524	0.8	45.3	58.0
6	0.552	0.530	0.7	46.0	65.3
7	0.563	0.535	0.7	48.0	71.3
8	0.575	0.541	0.7	49.6	70.8
9	0.587	0.547	0.7	50.2	72.5
10	0.599	0.552	0.7	51.7	70.2

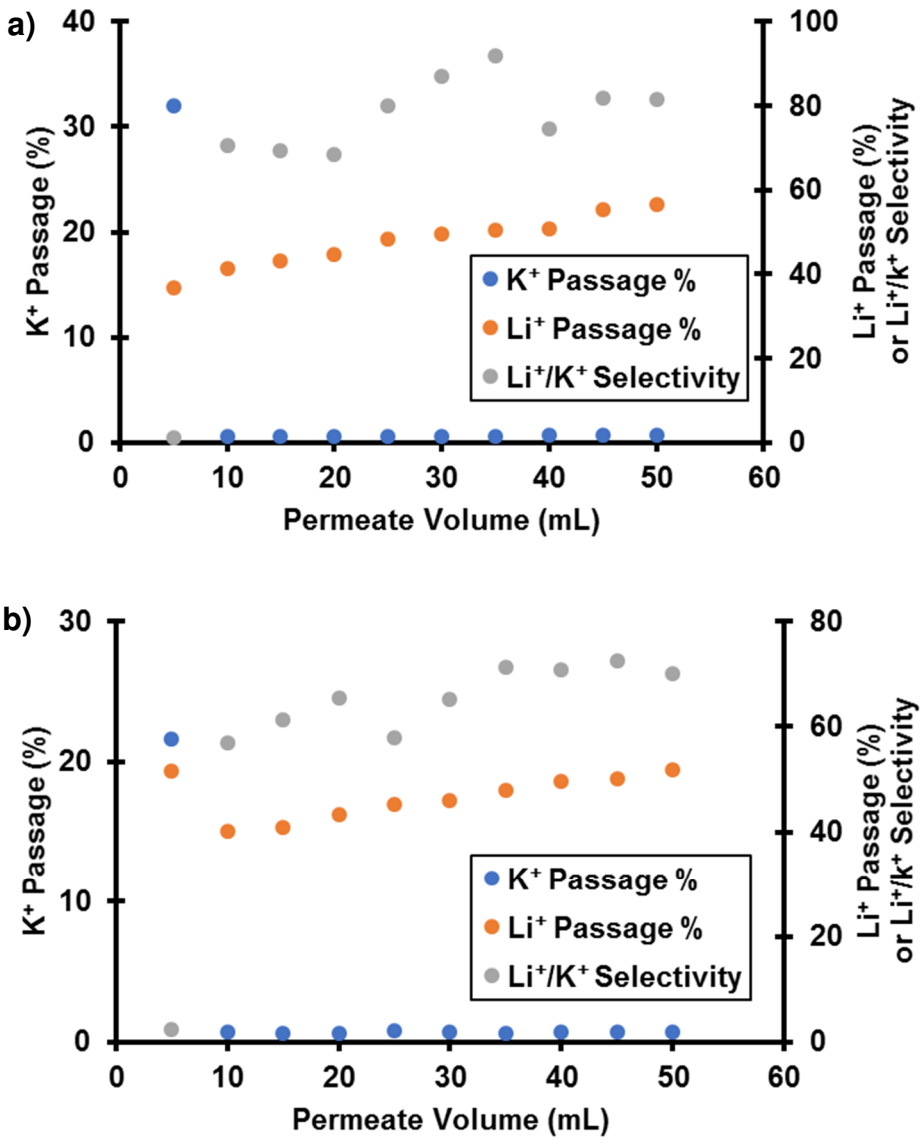

Figure S12. K^+ and Li^+ passages and Li^+/K^+ selectivities during flow through two different polycarbonate track-etched membrane samples (a and b) (nominal 10 nm pores) at 27.6 bar of transmembrane pressure. The feed initially contained a 0.5 mM LiOH, 0.5 mM KCl mixture. In typical experiments, we discard the first data point.

As shown in Table S11 and S12 and Figure S12, for membranes with 10 nm pores, K^+ passage remained steady over the course of the longer-term experiment, which lasted more than 3 hours for each membrane sample. In contrast, Li^+ passage increased primarily due to the increasing ionic strength and K^+/Li^+ ratio in the remaining feed solution. After the first 5 mL of permeate is discarded (which we did in typical experiments), the system reaches a pseudo steady state.

S3.5. Stationary membrane potential measurements

Table S13. Stationary membrane potential measurements with 3 different polycarbonate track-etched membranes (nominal 30 nm diameter pores).

Experiment	1	2	3
Source phase KCl concentration (mM)	1.414	1.414	1.414
Receiving phase KCl concentration (mM)	0.707	0.707	0.707
$(\phi^{S3} - \phi^{S2})$	15.2	16.4	15.6

We employed stationary membrane potential measurements to estimate the surface charge density. Table S13 presents the results. Using a model that incorporated solution non-ideality, impact of osmosis on the trans-membrane potential, and a numerical Poisson-Boltzmann simulation,[4] we estimated the surface charge density from the transmembrane potentials. This gives a value of -3.4 mC/m^2, which is similar to the value we employed in simulations for transport using a feed solution containing a mixture of 0.1 mM LiCl and 0.1 mM KCl. However, the measurements employed a higher salt concentration, which could affect the surface charge. Moreover, the model calculations do not account for the unstirred layers next to the membrane. A literature study gave a surface charge value of -3 mC/m^2 of the same membranes.[5]

S3.6. Pore density and pore size calculations

According to Tables S1 to S6, the measured average superficial velocity per bar of transmembrane pressure of the 30 nm membranes is 5.3 ± 0.6 µm/s/bar. According to Hagen–Poiseuille equation, the flow velocity per bar of transmembrane pressure within a 30 nm diameter pore should be 526.7 µm/s/bar. Dividing the average superficial velocity by 526.7 µm/s/bar gives a porosity (% of open area) of 1.0%. However, the manufacturer lists a pore density of 6×10^8 pores/cm^2, which corresponds to a porosity of 0.42% if the pore diameters are indeed 30 nm. If the nominal pore density is accurate, the actual effective diameter of the nominal 30 nm pores is 37 nm. In contrast, top-view SEM images show a pore size less than 37 nm, suggesting the pores could have a cigar-like shape.[6] The simulations in the main text employ the nominal 30 nm pore diameter. However, we briefly compared simulated K^+ and Li^+ passages for membranes with 30 and 37 nm pores (Figures S13 and S14). Employing a 37 nm pore diameter could make a small difference in calculated K^+ and Li^+ passages. However, the simulations with either pore size show the same trends.

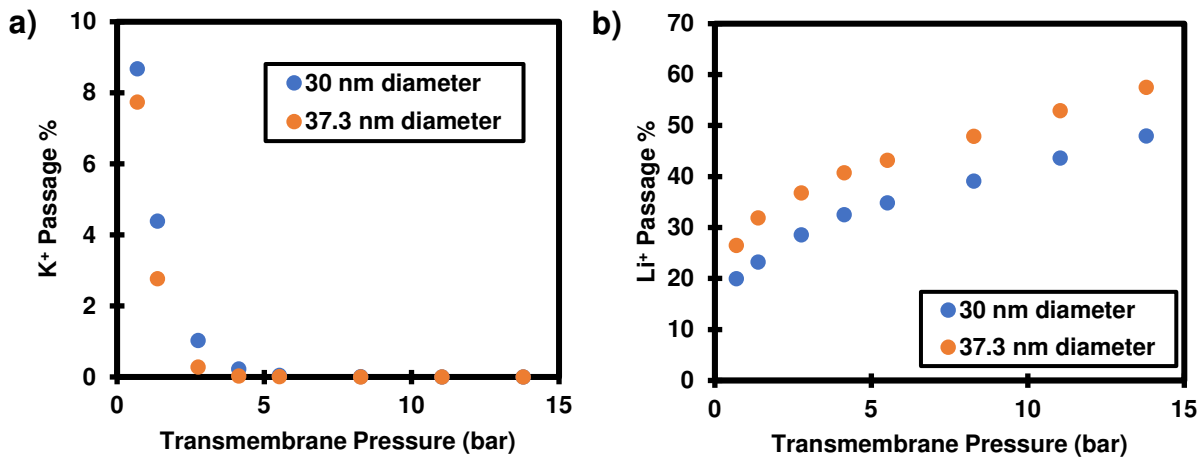

Figure S13. Simulated (a) K^+ and (b) Li^+ passages during flow through membranes with either 30 or 37 nm diameter pores at various transmembrane pressures. The feed contains a 0.1 mM LiCl, 0.1 mM KCl mixture. The simulation assumes an unstirred layer thickness of 10 µm and a surface charge density of -3 mC/m^2.

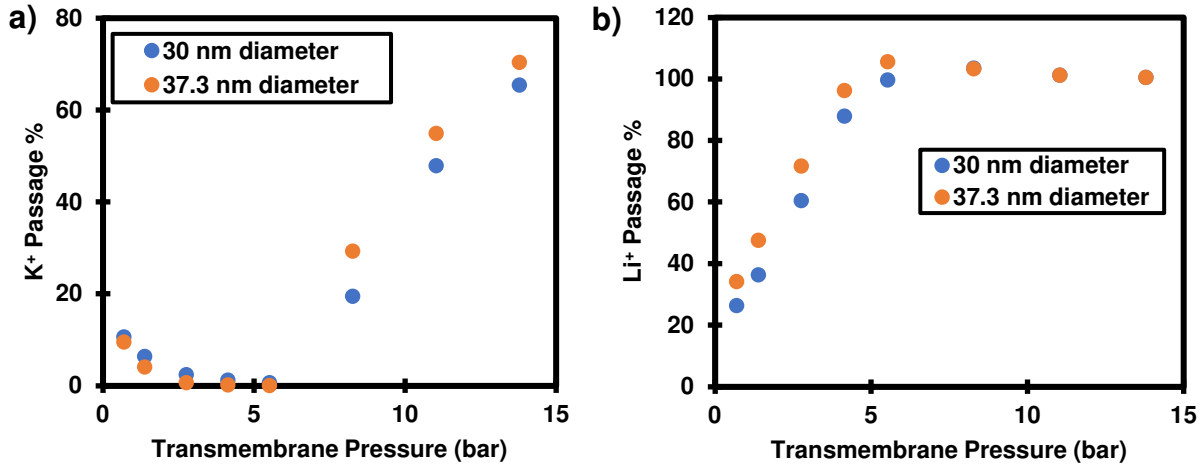

Figure S14. Simulated (a) K^+ and (b) Li^+ passages during flow through membranes with either 30 or 37 nm diameter pores at various transmembrane pressures. The feed contains a 0.1 mM LiCl, 0.1 mM KCl mixture. The simulation assumes an unstirred layer thickness of 75 µm and a surface charge density of -3 mC/m^2.

S4. Modelling rationale

S4.1. Homogenous approximation

In the homogenous model, we assume the negative charges on the membrane pore wall are homogeneously distributed within the pore to give a fixed charge concentration, c_x, described by equation (S7):

$$c_x = \left|\frac{2\pi r_p L\sigma}{\pi r_p^2 L}\right| = \left|\frac{2\sigma}{r_p}\right| \quad \text{(S7)}$$

In this equation, r_p, L, and σ are the radius, length, and surface charge density of the pore, respectively. For the polycarbonate membranes, σ is negative. This model also assumes that the flow velocity profile is homogenous (plug flow). Therefore, ion concentrations in the membrane, $c_{i,m}$, and flow velocity, $j_{v,m}$, are independent of radial coordinate, r.

$$\frac{dc_{i,m}}{dr} = \frac{dj_{v,m}}{dr} = 0 \quad \text{(S8)}$$

The homogenous model does not completely describe the physics of the system, as charges reside on the pore wall and the flow velocity should have a parabolic profile. However, this simplification greatly decreases the numerical calculations needed to determine the concentration profiles in the system, and the results from the homogenous model are very useful for providing initial guess values when solving the heterogeneous model described in section S4.2. Moreover, when the Debye length is larger than the pore radius, the concentration profiles in the two models are similar. All of the modelling results reported in this study come from the more rigorous heterogenous model.

The extended Nernst-Planck equation describes ion transport in the membrane:

$$j_{i,m} = -D_{i,m}\frac{dc_{i,m}}{dx} - z_i c_{i,m} D_{i,m}\frac{F}{RT}\frac{d\phi}{dx} + c_{i,m} j_{v,m} \quad \text{(S9)}$$

In the above equation, $j_{i,m}$, $D_{i,m}$, and z_i are the flux in the membrane pores, the diffusion coefficient in the membrane, and the charge of ion i, respectively. Additionally, ϕ is the electrostatic potential, $j_{v,m}$ is the flow velocity inside the pores, and F, R, and T are Faraday's constant, the gas constant, and temperature, respectively. The first term on the right-hand-side of the equation describes diffusive flux governed by Fick's law; the second term is electromigration flux, employing the Einstein–Smoluchowski relation; and the third term describes convective flux. For a system containing three ions (K^+, Li^+, and Cl^-), equation (S9) is a system of three equations, one for each ion (denoted as ion 1, 2, and 3):

$$j_{1,m} = -D_{1,m}\frac{dc_{1,m}}{dx} - z_i c_{1,m} D_{1,m}\frac{F}{RT}\frac{d\phi}{dx} + c_{1,m} j_{v,m} \quad \text{(S10)}$$

$$j_{2,m} = -D_{2,m}\frac{dc_{2,m}}{dx} - z_i c_{2,m} D_{2,m}\frac{F}{RT}\frac{d\phi}{dx} + c_{2,m} j_{v,m} \quad \text{(S11)}$$

$$j_{3,m} = -D_{3,m}\frac{dc_{3,m}}{dx} - z_3 c_{3,m} D_{3,m}\frac{F}{RT}\frac{d\phi}{dx} + c_{3,m} j_{v,m} \quad \text{(S12)}$$

Note that only two of the three equations and two of the three ion concentrations are independent due to the zero current $\left(\sum_i z_i j_{i,m} = 0\right)$ and electrical neutrality $\left(\sum_i z_i c_{i,m} = c_x; assumes\ negative\ fixed\ charge\right)$ conditions. Assuming electroneutrality and that the

membrane fixed charge concentration is the same everywhere $\left(\frac{dc_x}{dx} = 0\right)$, one can transform equations (S10-S12) into equations (S13-S15) by replacing the expression for $\frac{d\phi}{dx}$:

$$j_{1,m} = -D_{1,m}\frac{dc_{1,m}}{dx} + z_i c_{1,m} D_{1,m}\frac{\sum_i z_i \frac{j_{i,m}}{D_{i,m}} - j_{v,m}\sum_i z_i \frac{c_{i,m}}{D_{i,m}}}{\sum_i z_i^2 c_{i,m}} + c_{1,m} j_{v,m} \quad \text{(S13)}$$

$$j_{2,m} = -D_{2,m}\frac{dc_{2,m}}{dx} + z_i c_{2,m} D_{2,m}\frac{\sum_i z_i \frac{j_{i,m}}{D_{i,m}} - j_{v,m}\sum_i z_i \frac{c_{i,m}}{D_{i,m}}}{\sum_i z_i^2 c_{i,m}} + c_{2,m} j_{v,m} \quad \text{(S14)}$$

$$j_{3,m} = -D_{3,m}\frac{dc_{3,m}}{dx} + z_3 c_{3,m} D_{3,m}\frac{\sum_i z_i \frac{j_{i,m}}{D_{i,m}} - j_{v,m}\sum_i z_i \frac{c_{i,m}}{D_{i,m}}}{\sum_i z_i^2 c_{i,m}} + c_{3,m} j_{v,m} \quad \text{(S15)}$$

The equations above are equivalent to a system of three coupled ordinary differential equations:

$$\frac{dc_{1,m}}{dx} = -\frac{j_{1,m}}{D_{1,m}} + z_1 c_{1,m}\frac{z_1\frac{j_{1,m}}{D_{1,m}} + z_2\frac{j_{2,m}}{D_{2,m}} + z_3\frac{j_{3,m}}{D_{3,m}} - j_{v,m}z_1\frac{c_{1,m}}{D_{1,m}} - j_{v,m}z_2\frac{c_{2,m}}{D_{2,m}} - j_{v,m}z_3\frac{c_{3,m}}{D_{3,m}}}{z_1^2 c_{1,m} + z_2^2 c_{2,m} + z_3^2 c_{3,m}} + \frac{j_{v,m}}{D_{1,m}} c_{1,m} \quad \text{(S16)}$$

$$\frac{dc_{2,m}}{dx} = -\frac{j_{2,m}}{D_{2,m}} + z_2 c_{2,m}\frac{z_1\frac{j_{1,m}}{D_{1,m}} + z_2\frac{j_{2,m}}{D_{2,m}} + z_3\frac{j_{3,m}}{D_{3,m}} - j_{v,m}z_1\frac{c_{1,m}}{D_{1,m}} - j_{v,m}z_2\frac{c_{2,m}}{D_{2,m}} - j_{v,m}z_3\frac{c_{3,m}}{D_{3,m}}}{z_1^2 c_{1,m} + z_2^2 c_{2,m} + z_3^2 c_{3,m}} + \frac{j_{v,m}}{D_{2,m}} c_{2,m} \quad \text{(S17)}$$

$$\frac{dc_{3,m}}{dx} = -\frac{j_{3,m}}{D_{3,m}} + z_3 c_{3,m}\frac{z_1\frac{j_{1,m}}{D_{1,m}} + z_2\frac{j_{2,m}}{D_{2,m}} + z_3\frac{j_{3,m}}{D_{3,m}} - j_{v,m}z_1\frac{c_{1,m}}{D_{1,m}} - j_{v,m}z_2\frac{c_{2,m}}{D_{2,m}} - j_{v,m}z_3\frac{c_{3,m}}{D_{3,m}}}{z_1^2 c_{1,m} + z_2^2 c_{2,m} + z_3^2 c_{3,m}} + \frac{j_{v,m}}{D_{3,m}} c_{3,m} \quad \text{(S18)}$$

Again, only two of the equations are independent.

Similarly, we use the extended Nernst-Planck equation to describe ion transport in the unstirred layer next to the membrane:

$$j_i = -D_i\frac{dc_i}{dx} - z_i c_i D_i\frac{F}{RT}\frac{d\phi}{dx} + c_i j_v \quad \text{(S19)}$$

In equation (S19), j_i is the ion flux in the unstirred layer, D_i is the ion diffusion coefficient in solution, c_i is the ion concentration in solution, and j_v is the convective flow velocity inside the unstirred layer (or superficial velocity, v, in equation S3). Note that we assume that the distance between the membrane pores is much less than the thickness of the unstirred layers so flow and concentration profiles in the unstirred layer are essentially homogeneous above the membrane. We make this same assumption in both the homogeneous and heterogeneous models. Similar to the method for determining the concentration profile in the pores, we perform transformations to obtain a system of three coupled ordinary differential equations:

$$\frac{dc_1}{dx} = -\frac{j_1}{D_1} + z_1 c_1\frac{z_1\frac{j_1}{D_1} + z_2\frac{j_2}{D_2} + z_3\frac{j_3}{D_3} - j_v z_1\frac{c_1}{D_1} - j_v z_2\frac{c_2}{D_2} - j_v z_3\frac{c_3}{D_3}}{z_1^2 c_1 + z_2^2 c_2 + z_3^2 c_3} + \frac{j_v}{D_1} c_1 \quad \text{(S20)}$$

$$\frac{dc_2}{dx} = -\frac{j_2}{D_2} + z_2 c_2\frac{z_1\frac{j_1}{D_1} + z_2\frac{j_2}{D_2} + z_3\frac{j_3}{D_3} - j_v z_1\frac{c_1}{D_1} - j_v z_2\frac{c_2}{D_2} - j_v z_3\frac{c_3}{D_3}}{z_1^2 c_1 + z_2^2 c_2 + z_3^2 c_3} + \frac{j_v}{D_2} c_2 \quad \text{(S21)}$$

$$\frac{dc_3}{dx} = -\frac{j_3}{D_3} + z_3 c_3\frac{z_1\frac{j_1}{D_1} + z_2\frac{j_2}{D_2} + z_3\frac{j_3}{D_3} - j_v z_1\frac{c_1}{D_1} - j_v z_2\frac{c_2}{D_2} - j_v z_3\frac{c_3}{D_3}}{z_1^2 c_1 + z_2^2 c_2 + z_3^2 c_3} + \frac{j_v}{D_3} c_3 \quad \text{(S22)}$$

At the membrane/unstirred layer interface and membrane/permeate interface, we use Donnan equilibrium,[7] equation (S23), to describe ion partitioning.

$$\frac{c_{i,m,int}}{c_{i,int}} = exp\left(-\frac{z_i F \phi^{Donnan}}{RT}\right) \quad \text{(S23)}$$

In this equation, ϕ^{Donnan} is the Donnan potential difference at the membrane/solution interfaces where $c_{i,m,int}$ is the ion concentration just inside the membrane, and $c_{i,int}$ is the ion concentration just outside the membrane (in solution). In the solution and in the membrane, we assume electroneutrality:

$$\sum_i z_i c_i = 0 \qquad \sum_i z_i c_{i,m} = c_x \quad \text{(S24)}$$

Combining equations (S23) and (S24), one can solve for $\frac{c_{i,m,int}}{c_{i,int}}$ for all ions if we know the fixed charge concentration (the Donnan potential is same for all ions).

We solved equations (S16-S18 and S20-S22) numerically by guessing two ion fluxes (the third flux is specified by the zero-current condition $\left(\sum_i z_i j_{i,m} = 0\right)$), and consequently, guessing the permeate concentrations ($c_{i,permeate} = \frac{j_{i,m}}{j_{v,m}}$). To offer more clarity, equations (S20-S22) are essentially an initial-value problem with three coupled ordinary differential equations. Using the Donnan equilibrium and guessed permeate concentrations, one may calculate the ion concentrations just inside the membrane at the membrane/permeate interface. The calculated concentrations at the interface serve as initial conditions. A 4th-order Runge-Kutta method solves the concentration profiles in the membrane and one may use the Donnan equilibrium to solve the partitioning behavior at the membrane/unstirred layer interface. Equations (S16-S18), again, are an initial value problem that may be solved with ion concentrations just outside the membrane (calculated by Donnan equilibrium) as initial conditions. A 4th-order Runge-Kutta method solved the concentration profiles in the unstirred layer and calculated the feed concentrations from guessed fluxes. The calculated feed concentrations must converge to the experimental (or specified) values. We used an iterative procedure to vary two ion fluxes until the convergence occurred.

Table S14 lists the parameters used in the calculations. We calculated the flow velocity inside the membrane pores using the Hagen–Poiseuille equation:

$$j_{v,m} = \frac{\Delta P r_p^2}{8\eta L} \quad \text{(S25)}$$

In the above equation, ΔP is the transmembrane pressure, η is the solution dynamic viscosity, and r_p is the pore radius. At steady state, the ion flux multiplied by the area as well as the volumetric flow rate must be equal inside the membrane pores and in the unstirred layer. This leads to

$$j_v = \varepsilon j_{v,m} \quad \text{(S26)}$$

$$j_i = \varepsilon j_{i,m} \quad \text{(S27)}$$

In these equations, ε is the membrane porosity (defined as the membrane open area divided the total membrane area). The flow velocity within the unstirred layer, j_v, is measured experimentally (superficial normal velocity in Tables S1-S6) and the porosity is calculated using equations (S25) and (S26). Subsequently, we use equation (S27) to convert fluxes in the pore to fluxes in the

unstirred layer. SEM images (Figures S4 and S5) suggest that the pore diameter at the opening is close to the nominal value of 30 nm, so we use that value when calculating the flow velocity in the pores in equation (S25). The SEM image in Figure S6 shows that the membrane thickness is also close to the nominal value of 6 µm, so we use that value in equation (S25) and when solving the coupled differential equations.

So far, we described the homogenous transport-modelling rationale only for a three-ion system (K^+, Li^+, and Cl^-). However, this model also applies to more complicated systems such as a four-ion system (K^+, Li^+, Cl^-, and OH^-), which gives rise to 4 coupled ordinary differential equations (one for each ion, only three equations are independent). Thus, three ion fluxes must be iterated for convergence (instead of two). This is more numerically expensive but still possible.

As Table S14 shows, most of the parameters needed for the modelling come from literature values, well-known theories, or experimental measurements. However, there are a few assumptions and adjustable parameters. We assume the ion diffusion coefficients[8] are the same in the membrane and in solution. This is reasonable because the membrane pore diameter (30 nm) is much larger than the largest hydrated ion diameter (~0.5 nm for Li^+).[9] This leaves us with two uncertain parameters: surface charge density, σ (or fixed charge concentration, c_x, in the homogenous model), and the unstirred layer thickness. We chose a round value of σ that approximately fits the experimental K^+ passages at the lowest transmembrane pressure with a 10-µm unstirred layer. At this lowest pressure (or flow rate), the effect of concentration polarization is minimized. The selected values of σ also reasonably describe the Li^+ passages at the lowest pressures. Note that for solutions containing LiOH and KCl, the estimation of surface charge must use the four-ion model due to the presence of OH^- in the solution.

Table S14. Parameters used in the homogenous model

D_{K^+} ($m^2\ s^{-1}$)	1.96×10^{-9}
D_{Li^+} ($m^2\ s^{-1}$)	1.03×10^{-9}
D_{Cl^-} ($m^2\ s^{-1}$)	2.03×10^{-9}
D_{OH^-} ($m^2\ s^{-1}$)	5.27×10^{-9}
$D_{K^+,m}$ ($m^2\ s^{-1}$)	1.96×10^{-9}
$D_{Li^+,m}$ ($m^2\ s^{-1}$)	1.03×10^{-9}
$D_{Cl^-,m}$ ($m^2\ s^{-1}$)	2.03×10^{-9}
$D_{OH^-,m}$ ($m^2\ s^{-1}$)	5.27×10^{-9}
Membrane thickness, L (µm)	6
Unstirred layer thickness (µm)	Varied to examine its effect
Pore radius, r_p (nm)	15 (for 30 nm diameter pores)
Surface charge density, σ (mC/m^2)	-3 (for 0.1 mM KCl and 0.1 mM LiCl feed) -5 (for 0.1 mM KCl and 0.1 mM LiOH feed) -7 (for 0.5 mM KCl and 0.5 mM LiOH feed)
c_x (M)	Equation (S7)
Dynamic viscosity, η (Pa s)	0.00089
$j_{v,m}$ (µm/s)	Equation (S25)
j_v (µm/s)	Measured experimentally (Tables S1-S6)
$j_{i,m}$ ($mol/dm^2/s$)	Iterative parameters
j_i ($mol/dm^2/s$)	Equation (S27)

With values of surface charge in hand, we varied the unstirred layer thickness to examine its effect on ion passages. Importantly, we do not expect the model to fit the data perfectly but rather to demonstrate the trends in ion passage with varying unstirred layer thicknesses.

S4.2. Heterogeneous model of ion transport

This more rigorous model accounts for the radial dependence of ion concentration and flow velocity inside the membrane pores. We employ virtual solutions to model ion transport in this case, where a virtual solution is a solution that is in thermodynamic equilibrium with the real ion concentrations within the pore at a given axial coordinate.[10] This concept is hard to grasp, but it greatly simplifies the calculation because the virtual solution composition varies only with the axial coordinate. We provide a brief justification of this concept.

Because the virtual solution (at a particular axial position) is in equilibrium with the ions within the pore at that position, the ion electrochemical potentials are equal in the virtual solution and the pore.

$$\mu_i^o + RTln\bar{c}_i + z_iF\bar{\phi} = \mu_i^o + RTlnc_{i,m}(r) + z_iF\phi(r) \quad \text{(S28)}$$

In the above equation, μ_i^o is the standard chemical potential for ion i; $\bar{c}_i$ is the ion concentration in the virtual solution; $\bar{\phi}$ is the virtual electrostatic potential; $c_{i,m}$ is the real ion concentration within a membrane pore, which depends on radial coordinate, r; and ϕ is the real electrostatic potential within a pore, which varies radially as well. The above equation assumes all activity coefficients are unity. Defining a partition coefficient, $\Gamma_i(r)$, and rearrangement of equation S28 lead to the following equations:

$$\Gamma_i(r) = \frac{c_{i,m}(r)}{\bar{c}_i} \quad \text{(S29)}$$

$$\Gamma_i(r) = exp\left(\frac{-z_iF\phi'(r)}{RT}\right) \quad \text{(S30)}$$

$$\phi'(r) = \phi(r) - \bar{\phi} \quad \text{(S31)}$$

The electrochemical potential gradient as well as convection drive ion transport, as equation (S32) describes:

$$j_{i,m}(r) = -\frac{D_{i,m}}{RT}c_{i,m}(r)\frac{d}{dx}\left(\mu_i^o + RTlnc_{i,m}(r) + z_iF\phi(r)\right) + c_{i,m}(r)j_{v,m}(r) \quad \text{(S32)}$$

Combining equation (S32) with equations (S28) and (S29) gives:

$$j_{i,m}(r) = -\frac{D_{i,m}}{RT}\bar{c}_i\Gamma_i(r)\frac{d}{dx}(\mu_i^o + RTln\bar{c}_i + z_iF\bar{\phi}) + \bar{c}_i\Gamma_i(r)j_{v,m}(r) = D_{i,m}\Gamma_i(r)\frac{d\bar{c}_i}{dx} - z_iD_{i,m}\frac{F}{RT}\Gamma_i(r)\bar{c}_i\frac{d\bar{\phi}}{dx} + \bar{c}_i\Gamma_i(r)j_{v,m}(r) \quad \text{(S33)}$$

Equation (S33) relates ion flux with virtual concentration, virtual electrostatic potential, and partition coefficient, $\Gamma_i(r)$. Due to the heterogeneity, flux varies with radial coordinate as well. We can take the area-averaged value of flux and this leads to equation (S34):

$$\langle j_{i,m}\rangle = -D_{i,m}\langle\Gamma_i\rangle\frac{d\bar{c}_i}{dx} - z_iD_{i,m}\bar{c}_i\langle\Gamma_i\rangle\frac{F}{RT}\frac{d\bar{\phi}}{dx} + \langle j_{v,m}\Gamma_i\rangle\bar{c}_i \quad \text{(S34)}$$

In this equation, $\langle j_{i,m} \rangle$ is the area-averaged ion flux within a pore. $\langle \Gamma_i \rangle$ and $\langle j_{v,m} \Gamma_i \rangle$ are the area-averaged partition coefficient and the area-averaged product of flow velocity and partition coefficient as defined in equations (S35-S37):

$$\langle \Gamma_i \rangle = \int_{r=0}^{r=r_p} \frac{\Gamma_i(r)}{\pi r_p^2} 2\pi r dr \tag{S35}$$

$$j_{v,m}(r) = 2\langle j_{v,m} \rangle (1 - \frac{r^2}{r_p^2}) \tag{S36}$$

$$\langle j_{v,m} \Gamma_i \rangle = \int_{r=0}^{r=r_p} \frac{j_{v,m}(r)\Gamma_i(r)}{\pi r_p^2} 2\pi r dr \tag{S37}$$

In the above equations, $\langle j_v \rangle$ is the area-averaged flow velocity and r_p is the pore radius.

To calculate the partition coefficient, $\Gamma_i(r)$, using equation (S30) we employ the Poisson-Boltzmann expression, equation (S38), along with appropriate boundary conditions, equations (S39) and (S40), to determine ϕ'.

$$\frac{d^2\phi\prime}{dr^2} + \frac{1}{r}\frac{d\phi\prime}{dr} = -\frac{F}{\varepsilon_o \varepsilon_p} \sum_i \bar{c}_i z_i exp\left(\frac{-z_i F \phi\prime}{RT}\right) \tag{S38}$$

$$\frac{d\phi\prime}{dr}(r = 0) = 0 \tag{S39}$$

$$\frac{d\phi\prime}{dr}\left(r = r_p\right) = -\frac{\sigma}{\varepsilon_o \varepsilon_p} \tag{S40}$$

In these equations $\varepsilon_o \varepsilon_p$ is the dielectric permittivity of solution in the membrane pore.

Similar to the homogenous model, one can rewrite equation (S34) as a system of three coupled differential equations (one for each ion) with the condition of electrical neutrality in the virtual solution ($\sum_i z_i \bar{c}_i = 0$ and $\sum_i z_i \frac{d\bar{c}_i}{dx} = 0$). This leads to

$$\frac{d\bar{c}_1}{dx} = -\frac{\langle j_{1,m} \rangle}{D_{1,m}\langle \Gamma_1 \rangle} + z_1 \bar{c}_1 \frac{z_1 \frac{\langle j_{1,m} \rangle}{D_{1,m}\langle \Gamma_1 \rangle} + z_2 \frac{\langle j_{2,m} \rangle}{D_{2,m}\langle \Gamma_2 \rangle} + z_3 \frac{\langle j_{3,m} \rangle}{D_{3,m}\langle \Gamma_3 \rangle} - z_1 \frac{\langle j_{v,m}\Gamma_1 \rangle}{D_{1,m}\langle \Gamma_1 \rangle}\bar{c}_1 - z_2 \frac{\langle j_{v,m}\Gamma_2 \rangle}{D_{2,m}\langle \Gamma_2 \rangle}\bar{c}_2 - z_1 \frac{\langle j_{v,m}\Gamma_3 \rangle}{D_{3,m}\langle \Gamma_3 \rangle}\bar{c}_3}{z_1^2 \bar{c}_1 + z_2^2 \bar{c}_2 + z_3^2 \bar{c}_3} + \frac{\langle j_{v,m}\Gamma_1 \rangle}{D_{1,m}\langle \Gamma_1 \rangle}\bar{c}_1 \tag{S41}$$

$$\frac{d\bar{c}_2}{dx} = -\frac{\langle j_{2,m} \rangle}{D_{2,m}\langle \Gamma_2 \rangle} + z_2 \bar{c}_2 \frac{z_1 \frac{\langle j_{1,m} \rangle}{D_{1,m}\langle \Gamma_1 \rangle} + z_2 \frac{\langle j_{2,m} \rangle}{D_{2,m}\langle \Gamma_2 \rangle} + z_3 \frac{\langle j_{3,m} \rangle}{D_{3,m}\langle \Gamma_3 \rangle} - z_1 \frac{\langle j_{v,m}\Gamma_1 \rangle}{D_{1,m}\langle \Gamma_1 \rangle}\bar{c}_1 - z_2 \frac{\langle j_{v,m}\Gamma_2 \rangle}{D_{2,m}\langle \Gamma_2 \rangle}\bar{c}_2 - z_1 \frac{\langle j_{v,m}\Gamma_3 \rangle}{D_{3,m}\langle \Gamma_3 \rangle}\bar{c}_3}{z_1^2 \bar{c}_1 + z_2^2 \bar{c}_2 + z_3^2 \bar{c}_3} + \frac{\langle j_v \Gamma_2 \rangle}{D_2\langle \Gamma_2 \rangle}\bar{c}_2 \tag{S42}$$

$$\frac{d\bar{c}_3}{dx} = -\frac{\langle j_{3,m} \rangle}{D_{3,m}\langle \Gamma_3 \rangle} + z_3 \bar{c}_3 \frac{z_1 \frac{\langle j_{1,m} \rangle}{D_{1,m}\langle \Gamma_1 \rangle} + z_2 \frac{\langle j_{2,m} \rangle}{D_{2,m}\langle \Gamma_2 \rangle} + z_3 \frac{\langle j_{3,m} \rangle}{D_{3,m}\langle \Gamma_3 \rangle} - z_1 \frac{\langle j_{v,m}\Gamma_1 \rangle}{D_{1,m}\langle \Gamma_1 \rangle}\bar{c}_1 - z_2 \frac{\langle j_{v,m}\Gamma_2 \rangle}{D_{2,m}\langle \Gamma_2 \rangle}\bar{c}_2 - z_1 \frac{\langle j_{v,m}\Gamma_3 \rangle}{D_{3,m}\langle \Gamma_3 \rangle}\bar{c}_3}{z_1^2 \bar{c}_1 + z_2^2 \bar{c}_2 + z_3^2 \bar{c}_3} + \frac{\langle j_{v,m}\Gamma_3 \rangle}{D_{3,m}\langle \Gamma_3 \rangle}\bar{c}_3 \tag{S43}$$

Similarly, equations (S44-S46) describe the ion concentrations inside the unstirred layer. However, in the unstirred layer we assume that ion concentrations profiles and flow velocity are homogeneous and vary only along the x coordinate because the thickness of this layer is much greater than the distance between pores.

$$\frac{dc_1}{dx} = -\frac{j_1}{D_1} + z_1 c_1 \frac{z_1\frac{j_1}{D_1} + z_2\frac{j_2}{D_2} + z_3\frac{j_3}{D_3} - j_v z_1\frac{c_1}{D_1} - j_v z_2\frac{c_2}{D_2} - j_v z_3\frac{c_3}{D_3}}{z_1^2 c_1 + z_2^2 c_2 + z_3^2 c_3} + \frac{j_v}{D_1} c_1 \quad \text{(S44)}$$

$$\frac{dc_2}{dx} = -\frac{j_2}{D_2} + z_2 c_2 \frac{z_1\frac{j_1}{D_1} + z_2\frac{j_2}{D_2} + z_3\frac{j_3}{D_3} - j_v z_1\frac{c_1}{D_1} - j_v z_2\frac{c_2}{D_2} - j_v z_3\frac{c_3}{D_3}}{z_1^2 c_1 + z_2^2 c_2 + z_3^2 c_3} + \frac{j_v}{D_2} c_2 \quad \text{(S45)}$$

$$\frac{dc_3}{dx} = -\frac{j_3}{D_3} + z_3 c_3 \frac{z_1\frac{j_1}{D_1} + z_2\frac{j_2}{D_2} + z_3\frac{j_3}{D_3} - j_v z_1\frac{c_1}{D_1} - j_v z_2\frac{c_2}{D_2} - j_v z_3\frac{c_3}{D_3}}{z_1^2 c_1 + z_2^2 c_2 + z_3^2 c_3} + \frac{j_v}{D_3} c_3 \quad \text{(S46)}$$

At steady state, the volumetric flow rate as well as the product of ion flux and area must be equal inside the membrane pores and in the unstirred layer.

$$j_v = \varepsilon \langle j_{v,m} \rangle \quad \text{(S47)}$$

$$j_i = \varepsilon \langle j_{i,m} \rangle \quad \text{(S48)}$$

$$\langle j_{v,m} \rangle = \frac{\Delta P r_p^2}{8\eta L} \quad \text{(S49)}$$

The flow velocity within the unstirred layer, j_v, is measured experimentally and the porosity is calculated using equations (S47) and (S49). We then use equation (S48) to convert average fluxes in the pores to fluxes in the unstirred layer.

We solve equations (S41-S43) and (S44-S46) using the same method as for the homogenous model. In principal, using the Poisson-Boltzmann equation and Hagen–Poiseuille flow profile one should calculate $\langle \Gamma_i \rangle$ and $\langle j_{v,m}\Gamma_i \rangle$ at every step of the numerical integration. However, this is numerically expensive. We found that $\langle \Gamma_i \rangle$ and $\frac{\langle j_{v,m}\Gamma_i \rangle}{\langle j_{v,m} \rangle}$ are functions of only two variables, $\frac{\sigma F r_p}{\varepsilon_o \varepsilon_p RT}$ and $\frac{r_p}{\sqrt{\frac{\varepsilon_o \varepsilon_p RT}{F \sum_i z_i^2 \bar{c}_i}}}$:

$$\langle \Gamma_i \rangle = \langle \Gamma_i \rangle \left(\frac{\sigma F r_p}{\varepsilon_o \varepsilon_p RT}, \frac{r_p}{\sqrt{\frac{\varepsilon_o \varepsilon_p RT}{F \sum_i z_i^2 \bar{c}_i}}} \right) \quad \text{(S50)}$$

$$\frac{\langle j_{v,m}\Gamma_i \rangle}{\langle j_{v,m} \rangle} = \frac{\langle j_{v,m}\Gamma_i \rangle}{\langle j_{v,m} \rangle} \left(\frac{\sigma F r_p}{\varepsilon_o \varepsilon_p RT}, \frac{r_p}{\sqrt{\frac{\varepsilon_o \varepsilon_p RT}{F \sum_i z_i^2 \bar{c}_i}}} \right) \quad \text{(S51)}$$

We pre-calculate a 2-dimensional array for each $\langle \Gamma_i \rangle$ and $\frac{\langle j_{v,m}\Gamma_i \rangle}{\langle j_{v,m} \rangle}$ with respect to the two variables. At each integration step, the arrays were called, and we calculated $\langle \Gamma_i \rangle$ and $\frac{\langle j_{v,m}\Gamma_i \rangle}{\langle j_{v,m} \rangle}$ via interpolation.

S5. Modelling results

S5.1. Streaming potentials

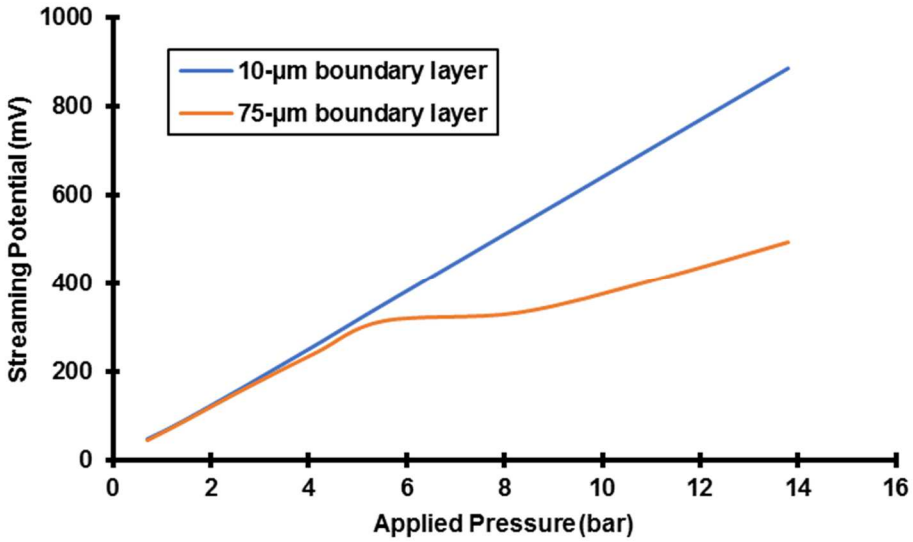

Figure S15. Simulated streaming potential drops inside a polycarbonate track-etched membrane (30 nm diameter pores) as a function of transmembrane pressure. The unstirred layer thickness is assumed to be either 10 or 75 µm. The feed contains a 0.1 mM LiCl, 0.1 mM KCl mixture. This is the real potential drop inside the pore only, it does not include the Donnan potentials at the interfaces of the membrane with unstirred (feed side) and permeate solutions.

Table S15. Simulated streaming potentials inside a polycarbonate track-etched membrane (30 nm diameter pores) as a function of transmembrane pressures. In addition to the results presented in Figure S15, this table also includes simulation results without any concentration polarization. This is the real potential drop inside the pore only, it does not include the Donnan potentials at the interfaces of the membrane with feed and permeate solutions.

Transmembrane pressure (bar)	Streaming potential (mv) (no concentration polarization)	Streaming potential (mv) (unstirred layer thickness = 10 µm)	Streaming potential (mv) (unstirred layer thickness = 75 µm)
0.7	47.1	46.6	44.2
1.4	85.6	85.0	83.6
2.8	172.5	171.0	165.1
4.2	262.2	259.8	241.9
5.5	352.6	351.4	313.4
8.3	533.5	530.2	332.4
11.0	714.5	708.6	406.2
13.8	895.5	886.7	493.0

S5.2 Convective and electromigration velocities

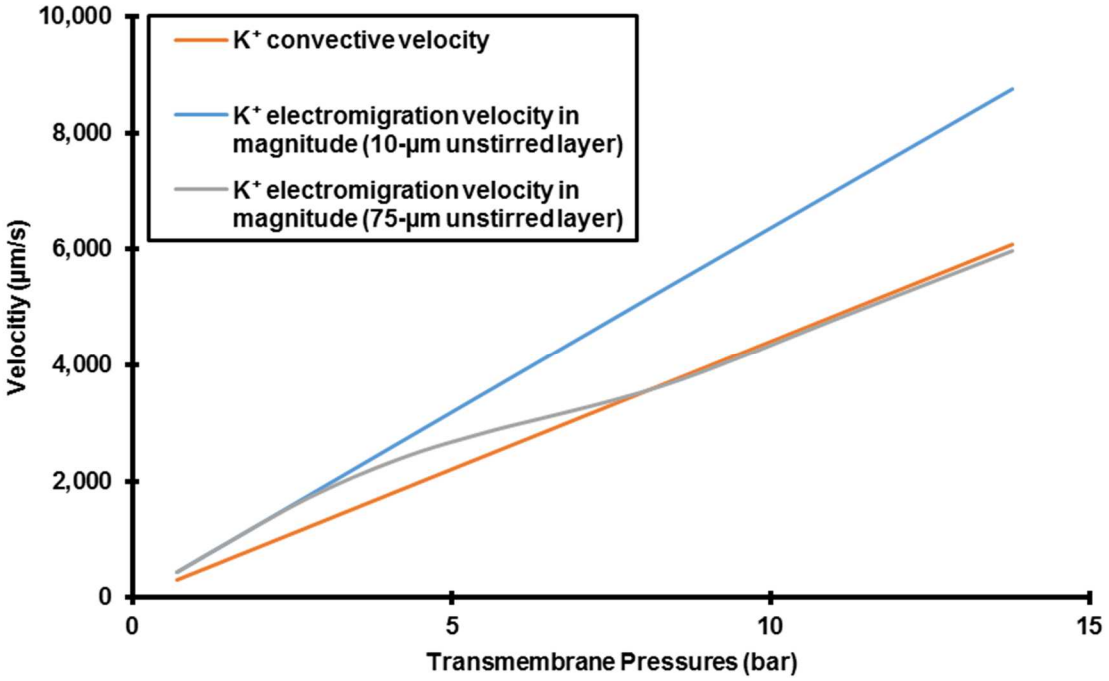

Figure S16. Simulated K^+ convective velocities and electromigration velocity magnitudes with a 10-µm or 75-µm unstirred layer. The transmembrane pressure varies from 0.7 to 13.8 bar. The simulation assumes a surface charge density of -3 mC/m^2. The feed contains a 0.1 mM LiCl, 0.1 mM KCl mixture. These are simulated velocities just inside the pore entrance. At higher pressures, the K^+ electromigration velocity does not exceed its convective velocity for a 75-µm unstirred layer due to concentration polarization.

S5.3. K^+ and Li^+ passages

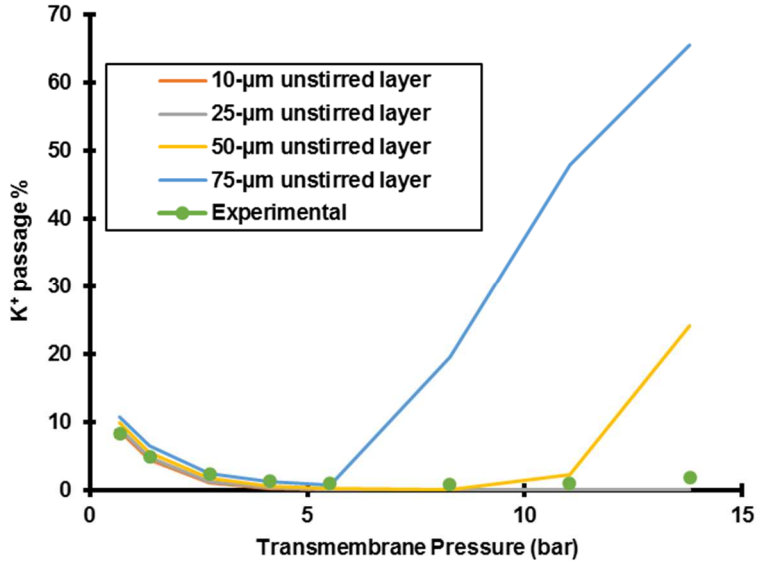

Figure S17. Simulated K^+ passages during flow of a 0.1 mM KCl, 0.1 mM LiCl mixture through a polycarbonate track-etched membrane (30 nm diameter pores) as a function of transmembrane pressure with various unstirred layer thicknesses. These simulations assume a surface charge density of -3 mC/m^2. This figure also shows experimental data. The data for the 10-μm unstirred layer are hidden by those for the 25-μm unstirred layer. Lines simply connect points to simplify the plot.

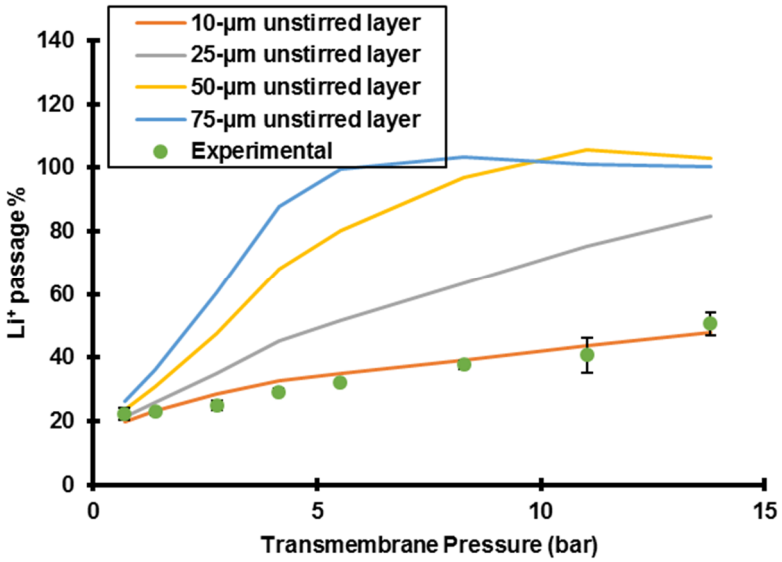

Figure S18. Simulated Li^+ passages during flow of a 0.1 mM KCl, 0.1 mM LiCl mixture through a polycarbonate track-etched membrane (30 nm diameter pores) as a function of transmembrane pressure with various unstirred layer thicknesses. These simulations assume a surface charge density of -3 mC/m^2. This figure also shows experimental data. Lines simply connect points to simplify the plot.

Table S16. Simulated K^+ and Li^+ passages through a polycarbonate track-etched membrane (30 nm diameter pores) as a function of transmembrane pressure. The feed contained a 0.1 mM KCl, 0.1 mM LiCl mixture, and we assumed various unstirred layer thicknesses as well as a surface charge density of -3 mC/m^2.

Transmembrane pressure (bar)	Unstirred layer thickness (μm)	K^+ passage %	Li^+ passage %
0.7	0	8.4	19.2
1.4		4.1	21.6
2.8		0.9	24.7
4.2		0.2	25.4
5.5		0.03	25.6
8.3		0.001	25.6
11.0		0.00005	25.6
13.8		0.000002	25.6
0.7	10	8.7	20.0
1.4		4.4	23.3
2.8		1.0	28.6
4.2		0.2	32.6
5.5		0.05	34.9
8.3		0.002	39.1
11.0		0.00008	43.7
13.8		0.000004	48.0
0.7	25	9.1	21.4
1.4		4.8	26.0
2.8		1.2	35.1
4.2		0.3	45.2
5.5		0.1	51.6
8.3		0.004	63.5
11.0		0.0002	75.2
13.8		0.00002	84.6
0.7	50	9.9	23.8
1.4		5.6	30.9
2.8		1.7	47.5
4.2		0.6	68.2
5.5		0.2	80.0
8.3		0.02	96.9
11.0		2.3	105.6
13.8		24.1	103.0
0.7	75	10.7	26.4
1.4		6.4	36.3
2.8		2.4	60.5
4.2		1.3	87.8
5.5		0.7	99.6
8.3		19.5	103.5
11.0		47.9	101.2
13.8		65.5	100.4

Table S17. Simulated K^+ and Li^+ passages through a polycarbonate track-etched membrane (30 nm diameter pore) as a function of transmembrane pressure. The feed contained a 0.1 mM KCl, 0.1 mM LiOH mixture, and we assumed various unstirred layer thicknesses as well as a surface charge density of -5 mC/m^2.

Transmembrane pressure (bar)	Unstirred layer thickness (μm)	K^+ passage %	Li^+ passage %
0.7	0	8.5	18.1
1.4		4.2	19.3
2.8		1.1	22.1
4.2		0.2	22.9
5.5		0.1	23.1
8.3		0.003	23.1
11.0		0.0001	23.1
13.8		0.000006	23.1
0.7	10	8.7	18.7
1.4		4.4	20.6
2.8		1.2	24.8
4.2		0.3	28.2
5.5		0.1	29.7
8.3		0.003	32.6
11.0		0.0002	36.2
13.8		0.00001	40.0
0.7	75	10.1	23.4
1.4		6.0	30.4
2.8		2.2	48.0
4.2		1.1	73.9
5.5		0.4	84.2
8.3		0.1	97.5
11.0		22.4	97.8
13.8		46.8	97.0

Table S18. Simulated K^+ and Li^+ passages through a polycarbonate track-etched membrane (30 nm diameter pore) as a function of transmembrane pressure. The feed contained a 0.5 mM KCl, 0.5 mM LiOH mixture, and we assumed various unstirred layer thicknesses as well as a surface charge density of -7 mC/m^2.

Transmembrane pressure (bar)	Unstirred layer thickness (μm)	K^+ passage %	Li^+ passage %
0.7	0	32.1	60.8
1.4		18.5	65.3
2.8		6.4	75.6
4.2		2.0	79.8
5.5		0.6	81.2
8.3		0.05	81.7
11.0		0.004	81.7
13.8		0.0003	81.8
0.7	10	32.7	62.0
1.4		19.4	67.6
2.8		7.3	80.5
4.2		2.7	88.7
5.5		0.9	92.6
8.3		0.1	97.2
11.0		0.01	100.8
13.8		0.001	104.3
0.7	75	36.8	69.1
1.4		26.1	80.4
2.8		17.5	99.7
4.2		26.4	105.6
5.5		38.4	103.6
8.3		60.3	100.4
11.0		74.9	99.3
13.8		84.6	99.0

S5.4. Effect of concentration polarization on Li^+ passage

As Table S16 shows, in the absence of concentration polarization the Li^+ passage asymptotically approaches a limiting value with increasing flow rate (or transmembrane pressure). However, at the highest pressure the Li^+ passage increases from 25.6% with no concentration polarization to 48% with only a 10-μm unstirred layer. In the main text, we argue that this occurs because concentration polarization increases the K^+/Li^+ ratio in the membrane and decreases anion exclusion to decrease streaming potentials. However, as Table S15 shows, the difference in the streaming potential (inside the membrane only) for a 10-μm unstirred layer and for no concentration polarization is only 1% at the highest flow rate (886.7 mV versus 895.5 mV). How could a 1% decrease in streaming potential (due to concentration polarization) account for nearly doubling the Li^+ passage?

At high flow rates, the diffusion flux is small compared to the electromigration and convection fluxes. This simplifies the extended Nernst-Planck relation to equation (S52), which allows us to better understand the Li^+ transport.

$$j_{Li^+,m} \xrightarrow[j_{v,m}\to\infty]{} c_{Li^+,m}(j_{v,m} - \frac{D_{Li^+,m}F}{RT}\frac{d\phi}{dx}) \tag{S52}$$

In this equation, $c_{Li^+,m}$ is the ion concentration inside the membrane. (At high flow rates the Li^+ concentration in the membrane is essentially a constant except near the pore entrance, see Figure 5 in the main text). We can calculate the permeate concentration as the ion flux divided by the convective velocity.

$$c_{Li^+,permeate} = \frac{j_{Li^+,m}}{j_{v,m}} \xrightarrow[j_{v,m}\to\infty]{} c_{Li^+,m}(1 - \frac{D_{Li^+,m}F}{j_{v,m}RT}\frac{d\phi}{dx}) \tag{S53}$$

Without concentration polarization, the Li^+ passage is 25.6% at the highest flow rate and K^+ passage is essentially 0. Due to the significant exclusion of anions, this means that $c_{Li^+,m}$ is nearly equal to the fixed charge concentration, c_x.

$$c_{Li^+,permeate} = \frac{j_{Li^+,m}}{j_{v,m}} \xrightarrow[j_{v,m}\to\infty]{} c_x(1 - \frac{D_{Li^+,m}F}{j_{v,m}RT}\frac{d\phi}{dx}) = 0.256c_{Li^+,feed} \tag{S54}$$

$$\frac{D_{Li^+,m}F}{j_{v,m}RT}\frac{d\phi}{dx} = 1 - \frac{0.256c_{Li^+,feed}}{c_x} \tag{S55}$$

For a negatively charged 30 nm diameter pore with a surface charge density of -3 mC/m^2, the fixed charge "concentration" is around 4 mM (equation S7).

$$\frac{D_{Li^+,m}F}{j_{v,m}RT}\frac{d\phi}{dx} = 1 - \frac{0.256\times 0.1\ mM}{4\ mM} = 0.9936 \tag{S56}$$

Note that $\frac{D_{Li^+,m}F}{j_{v,m}RT}\frac{d\phi}{dx}$ is nearly 1, and that the permeate concentration is proportional to $1 - \frac{D_{Li^+,m}F}{j_{v,m}RT}\frac{d\phi}{dx}$, or the fraction of the convective flux compensated by the electromigration flux. On going from no concentration polarization to a 10-μm unstirred layer, the streaming potential decreases by 1%, so we assume that $\frac{d\phi}{dx}$ decreases by 1% as well. Hence, with concentration polarization

$\frac{D_{Li^+,m}F}{j_{v,m}RT}\frac{d\phi}{dx} = 0.9936 \times 0.99 = 0.983664$ (with a 10-μm unstirred layer) (S57)

We can calculate the Li^+ passage again with the decreased electric field.

$$\frac{c_{Li^+,permeate}}{c_{Li^+,feed}} = \frac{c_x\left(1-\frac{D_{Li^+,m}F}{j_{v,m}RT}\frac{d\phi}{dx}\right)}{c_{Li^+,feed}} = \frac{4\ mM\times(1-0.983664)}{0.1\ mM} = 0.653 = 65.3\% \quad \text{(S58)}$$

Although this is an approximation, it shows that a small change in streaming potential has a large effect on Li^+ passage. In summary, due to high anion exclusion and low K^+ passage, the Li^+ concentration in much of the membrane is essentially equal to the "concentration" of the fixed charge. To maintain zero current the electromigration velocity of Li^+ opposes its convective velocity, and the magnitude of the convective velocity is only 1% greater than the magnitude of the electromigration velocity. Thus, even a 1% decrease in the electromigration velocity due to a 1% drop in streaming potential can greatly increase the Li^+ passage.

S5.5. Effect of pore size on Li^+/K^+ separations

As mentioned in the main text, smaller pores may prove useful in Li^+/K^+ separations at higher ionic strengths. The double-layer overlap is much greater in small pores than in larger ones, which induces stronger anion exclusion in smaller negatively charged pores. At the same flow velocity, streaming potentials are stronger as the pore diameter decreases, and this tends to make the magnitude of K^+ electromigration greater than its convection to give large Li^+/K^+ selectivities. To demonstrate this effect, we simulated K^+/Li^+ separations with a feed mixture of 1 mM KCl and 1 mM LiCl with flow through 10 nm or 30 nm diameter pores (Figure S19). Since we are only interested in the effect of pore size for now, we ignore concentration polarization in this section. Equation (S25) describes the flow velocity within the pores, and we use a membrane thickness of 6 µm.

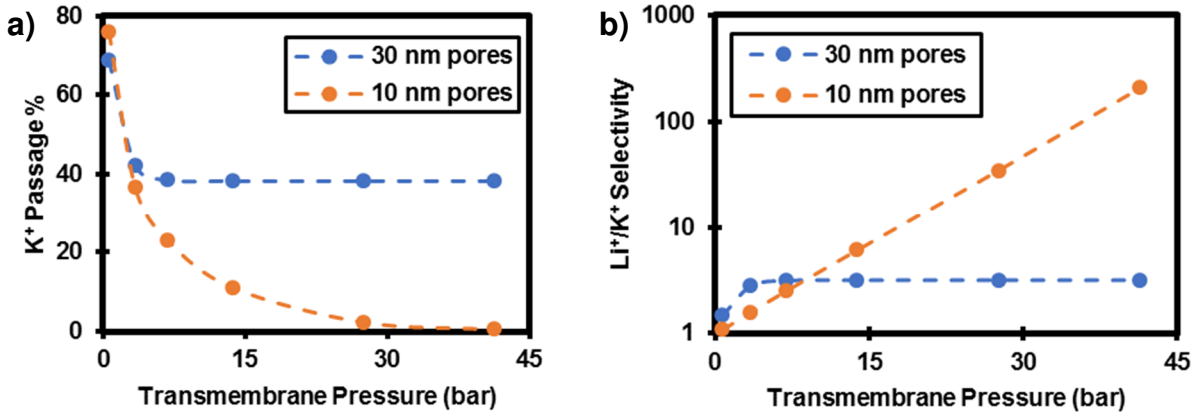

Figure S19. Simulated (a) K^+ passages and (b) Li^+/K^+ selectivities during flow of a 1 mM KCl, 1 mM LiCl mixture through track-etched membranes containing either 10 or 30 nm diameter pores using various transmembrane pressures. The surface charge density is assumed to be -3 mC/m^2 for all membranes. The membranes are 6-µm thick, and the flow velocities within the pores are calculated using equation (S25).

As Figure S19 shows, separation of K^+ and Li^+ with high selectivities is not possible with 30 nm pores under these conditions. The K^+ passage asymptotically approaches 38%. The streaming potentials within the 30 nm pores are not strong enough for the magnitude of K^+ electromigration to exceed its convection, regardless of transmembrane pressure. However, 10 nm pores can yield exceptionally high Li^+/K^+ selectivities, although the transmembrane pressure must be high.

If the membranes have the same pore density, membranes with 10 nm pores certainly have less throughput compared to 30 nm pore membranes. One should be aware that although smaller pore sizes may be useful in Li^+/K^+ separations at higher ionic strength, the throughput is certainly sacrificed. However, concentration polarization would be more pronounced with the 30 nm pores because of a higher superficial velocity at the same transmembrane pressure. Higher pore densities will also increase concentration polarization.

S5.6. Effect of surface charge density on Li^+/K^+ separations

As described in the previous section, for a 1 mM KCl, 1 mM LiCl feed mixture, simulations indicate it is not possible to separate K^+ and Li^+ with high selectivities using membranes with 30 nm pores with a surface charge density of -3 mC/m^2. However, a higher magnitude of surface charge density may give rise to stronger streaming potentials due to more extensive anion exclusion. To examine the effect of surface charge density, we simulated K^+/Li^+ separations with flow of a feed mixture of 1 mM KCl and 1 mM LiCl through 30 nm diameter pores containing various surface charge densities (Figure S20). Again, we ignore concentration polarization in this section.

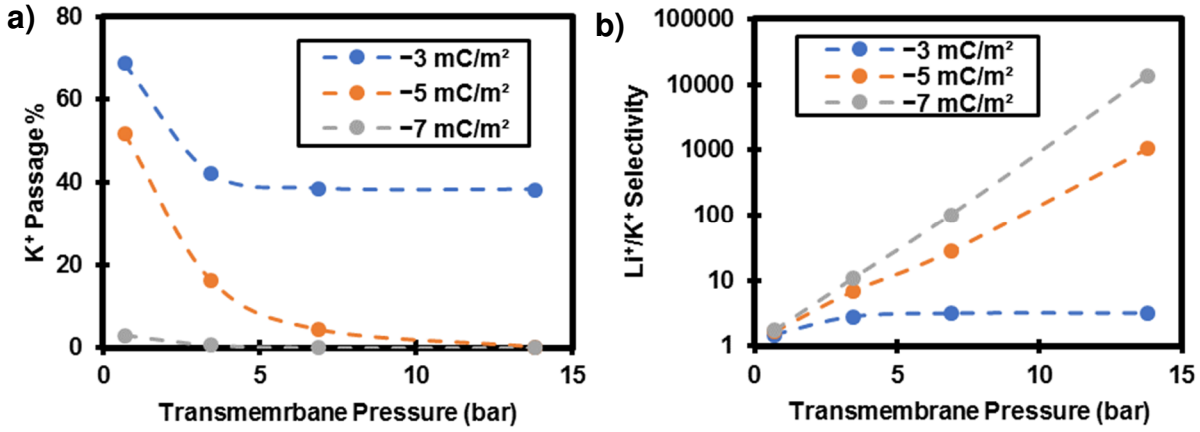

Figure S20. Simulated (a) K^+ passages and (b) Li^+/K^+ selectivities during flow of a 1 mM KCl, 1 mM LiCl mixture through track-etched membranes containing 30 nm diameter pores using various transmembrane pressures. The surface charge density varies from -3 mC/m^2 to -7 mC/m^2. The membranes are 6-µm thick. The flow velocities within the pores are calculated using equation (S25).

Remarkably, Li^+/K^+ selectivities increase dramatically on going from a surface charge density of -3 to -5 mC/m^2. This occurs because at -5 mC/m^2 the K^+ electromigration velocity exceeds its convective velocity due to more extensive anion exclusion. Selectivity increases even more as the surface charge density becomes more negative to further exclude anions. Of course, concentration polarization will decrease selectivities at high flow rates.

S6. Glossary and symbols

A	Active membrane area
c_i	Ion concentration in the unstirred layer
$c_{i,Feed}$	Feed concentration of ion i
$c_{i,Permeate}$	Permeate concentration of ion i
$c_{i,m}$	Ion concentration in the membrane pore
$\overline{c_i}$	Ion concentration in the virtual solution
c_x	Fixed charge concentration
D_i	Ion diffusion coefficient in the solution
$D_{i,m}$	Ion diffusion coefficient in the membrane pore
F	Faraday's constant
$j_{i,m}$	Ion flux in the membrane pore
$\langle j_{i,m} \rangle$	Area-averaged ion flux in the membrane pore
j_i	Ion flux in the unstirred layer
$j_{v,m}$	Flow velocity in the membrane pore
$\langle j_{v,m} \rangle$	Area-averaged flow velocity in the membrane pore
j_v	Flow velocity in the unstirred layer
L	Membrane thickness
ΔP	Transmembrane pressure
r	Radial coordinate
r_p	Pore radius
R	Gas constant
t	Time to collect 5 mL of permeate
T	Temperature
V_p	Permeate volume
x	Coordinate either in membrane or in unstirred layer
z_i	Ion charge
η	Dynamic viscosity
ε	Membrane porosity
ε_o	Permittivity of free space
ε_p	Dielectric constant of solvent in a pore
Γ_i	Ion partition coefficient
u_i	Ion electrophoretic mobility
ϕ	Electrostatic potential
$\bar{\phi}$	Virtual electrostatic potential
ϕ'	Electrostatic potential difference between ϕ and $\bar{\phi}$
ϕ^{Donnan}	Donnan potential difference at the membrane interfaces
σ	Surface charge density

References:

1 J. A. Armstrong, E. E. L. Bernal, A. Yaroshchuk, and M. L. Bruening, *Langmuir,* **2013**, *29*, 10287-10296.
2 C. P. Koutsou, and A. J. Karabelas, *Journal of Membrane Science,* **2012**, *399-400*, 60-72.
3 C. Cheng, A. Yaroshchuk, and M. L. Bruening, *Langmuir,* **2013**, *29*, 1885-1892.
4 A. Yaroshchuk, and M. P. Bondarenko, *Small,* **2018**, *14*, 1703723.
5 C. Lettmann, D. Möckel, and E. Staude, *Journal of Membrane Science,* **1999**, *159*, 243-251.
6 P. Y. Apel, I. V. Blonskaya, S. N. Dmitriev, O. L. Orelovitch, and B. Sartowska, *Journal of Membrane Science,* **2006**, *282*, 393-400.
7 F. G. Donnan, *Chemical Reviews,* **1924**, *1*, 73-90.
8 P. Vanýsek, in *CRC Handbook of Chemistry and Physics, 100th Edition (Internet Version 2019)* (Ed.: J. R. Rumble), CRC Press/Taylor & Francis, Boca Raton, FL.
9 P. Dechadilok, and W. M. Deen, *Industrial & Engineering Chemistry Research,* **2006**, *45*, 6953-6959.
10 A. Yaroshchuk, M. L. Bruening, and E. Zholkovskiy, *Advances in Colloid and Interface Science,* **2019**, *268*, 39-63.